



Numerical modelling of the muddy layer effect on Ship's resistance and squat

Sami Kaidi, Emmanuel Lefrançois, Hassan Smaoui

► To cite this version:

Sami Kaidi, Emmanuel Lefrançois, Hassan Smaoui. Numerical modelling of the muddy layer effect on Ship's resistance and squat. Ocean Engineering, 2020, 199, pp.106939. 10.1016/j.oceaneng.2020.106939 . hal-02464217

HAL Id: hal-02464217

<https://hal.utc.fr/hal-02464217>

Submitted on 7 Mar 2022

HAL is a multi-disciplinary open access archive for the deposit and dissemination of scientific research documents, whether they are published or not. The documents may come from teaching and research institutions in France or abroad, or from public or private research centers.

L'archive ouverte pluridisciplinaire **HAL**, est destinée au dépôt et à la diffusion de documents scientifiques de niveau recherche, publiés ou non, émanant des établissements d'enseignement et de recherche français ou étrangers, des laboratoires publics ou privés.



Distributed under a Creative Commons Attribution - NonCommercial 4.0 International License

NUMERICAL MODELLING OF THE MUDDY LAYER EFFECT ON SHIP'S RESISTANCE AND SQUAT

Sami Kaidi, CEREMA-DtecEMF, Margny les Compiègne, France ;

Emmanuel Lefrançois, Université de technologie de Compiègne Sorbonne universités, laboratoire Roberval FRE 2012 CNRS, France ;

Hassan Smaoui, CEREMA-DtecEMF, Margny les Compiègne, France ;

ABSTRACT

The increasing use of maritime transport has led to an increase in ship size. However, the dimensions of channels and harbours cannot follow the expansion rate of ships. Large ships will experience shallow water effects such as the bottom effect more severely, which plays an important role in the manoeuvrability and the stability of ships. To reduce navigational restriction in estuary environment and close to ports (see Figure 1), the World Association for Waterborne Transport Infrastructure (PIANC) established the concept of the nautical bottom. Using this concept, ships can navigate with both small and negative under keel clearance (UKC) relative to the water-mud interface. Hence, the aim of this work, is to conduct a numerical investigation in order to study the influence of the muddy seabed on the ship's manoeuvrability especially on the ship's resistance and squat. Accordingly, a 3D Computational Fluid Dynamics (CFD) model based on the Volume of Fluid (VoF) method was used to simulate the multiphase flow for various setups. Four parameters were tested: the mud properties, the ship's speed, the mud thickness and the UKC value relative to the water-mud interface. The numerical results of this investigation were in reasonable agreement with experimental data. Through this investigation it was also shown the performances of the CFD method to simulate setups difficult to achieve in towing tank.



Figure 1. Ship sailing in the Gironde estuary.

NOMENCLATURE

| | |
|------------------|---|
| α_p | Volume fraction |
| B | Ship's beam (m) |
| C_B | Ship's block coefficient |
| Fn | Froude number |
| Fn_i | Internal Froude number |
| h | Total depth (m) (water + mud) |
| h_w | Water depth (m) |
| hm | Mud thickness (m) |
| K | Consistency factor ($\text{Kg.s}^n/\text{m}$) |
| L_{OA} | Ship's Length over all (m) |
| L_{PP} | Ship's length between perpendiculars (m) |
| n | Power law exponent |
| T | Ship's draft (m) |
| t | Time (s) |
| p | Fluid pressure (Pa) |
| p' | Fluctuation of the fluid pressure (Pa) |
| UKC | Under Keel Clearance (m) |
| \mathbf{u} | Fluid velocity vector (m/s) |
| \mathbf{u}' | Fluctuation of the fluid velocity vector (m/s) |
| V_s | Ship speed (m/s) |
| η | Dynamic viscosity (Pa.s) |
| ρ_w | Water density (kg/m^3) |
| ρ_m | Mud density (kg/m^3) |
| $\dot{\gamma}$ | Shear rate ($1/\text{s}$) |
| $\dot{\gamma}_c$ | Critical shear rate ($1/\text{s}$) |
| τ | Shear stress (Pa) |
| τ_0 | Yield stress (Pa) |

1 INTRODUCTION

Any ship navigating through confined and shallow waters is strongly affected by hydrodynamic effects, as opposed to in open seas. Major effects of the limited navigating width and water depth (h) are the squat effect, and the increase in the ship's resistance. Water in front of the bow is pushed away, and flows down to the sides and under the hull of the ship with an increased velocity (See Figure 2) due to the reduced section. According to Bernoulli's principle, increasing velocity under the hull indicates a vertical pressure drop, and consequently the ship's sinkage increases. In addition, the ship generally trims forward or aft, as the bow or stern may experience more or less pressure drop, depending on the ship type. The effects of sinkage and trim are known as the ship's squat. This has a significant influence on the ship's resistance and can lead to serious safety issues, such as grounding, loss of steering, or collision.

In estuaries, the presence of the mud layer can significantly modify the ship's behaviour, especially when the ship is navigating in negative UKC relative to the mud/water interface. Note that the concept of the nautical bottom was established by the PIANC MarCom Working Group 30 in their 2014 report. This concept enables ships with larger drafts

whose physical properties do not exceed the critical limit (whereby contact with the ship's keel causes damage or unacceptable effects on controllability and manoeuvrability) to navigate in the mud layer. The same report also noted that it is difficult to give the critical limit value, hence, different density limits were set for different ports. That said, a critical limit was still provided, based only on the mud density, where the nautical bottom is the level from where the mud density is more than 1200 kg/m^3 . The viscosity of the mud could not be used as a parameter to define the nautical bottom because it changes under shear rates change. In some ports, such as the Port of Emden, Germany, the critical limit is given as a yield point that has been fixed to 100 Pa (Wurpts, 2005). Using this criterion, it was observed that the corresponding bottom density (approximately 1300 kg/m^3) considerably exceeded the limit given by PIANC.

In the Gironde estuary, the squat is an essential parameter for the traffic management of ships, where the water level in the estuary depends on the tide. Accordingly, to accommodate larger ships it is necessary to wait until the tide is high. Ships have to sail at the same speed as the propagation of the tide wave, which is in the order of 10 kn. However, this is not always the case, because in some situations ships can no longer keep up with the speed of the tidal wave for various reasons (mainly related to the significant increase in the ship's resistance caused by the ship's squat in the mud, which slows its speed considerably). In other situations, ships are equipped with a power limiter that stops the operation of the propulsive system if the ship meets a strong resistance. In such a situation, ships will be moored to wait for the next tide. To manage the estuarine network better, and to ensure safe navigation, it is thus essential to study the phenomenon of ship's resistance, its origins, and any consequences for navigation.

To predict a ship's squat, several empirical formulas have previously been proposed. Barrass and Derrett (1999) concluded some important factors of the squat effect, as follows:

- The main factor is the ship speed relative to the water, and the squat is approximately proportional to the square of this velocity;
- The decrease of water depth will increase the ship's squat;
- The block coefficient of the ship (that is the ratio of the ship's underwater volume to the volume of box surrounding it) is proportional to the squat;
- Similarly, the blockage factor (a ratio of the ship's immersed cross section to that of the canal) has a direct impact on the squat.

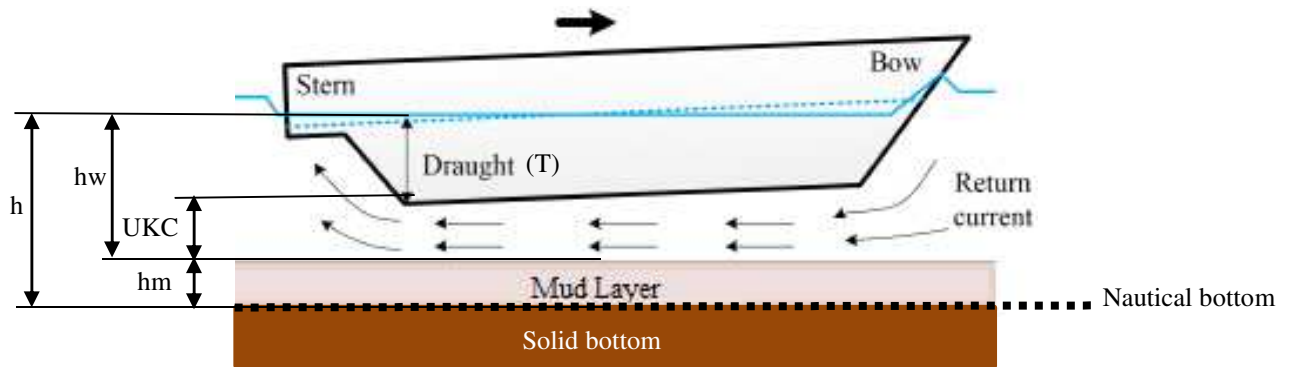


Figure 2. Nautical bottom representation with flow around a ship.

Over time, numerical efforts have been focused on estimating ship's resistance and squat. The slender-body method assumes that a ship's beam, free surface wave amplitude, and water depth are small compared to its length. This allows the simplification of the flow simulation in two dimensions using the slender-body theory (Gourlay, 2008; Tuck, 1964). To take into account the dynamic coupling of a ship's motion with flow, the potential flow theory can be applied, which only assumes the flow to be irrotational. This has been widely used for squat prediction and very good results have been obtained (Debaillon, 2010; Ma et al., 2016; Sergent et al., 2015), whereas it is difficult to apply the potential flow model to resistance prediction, because it neglects the viscous stresses, crucial for evaluating the ship's resistance.

Modern CFD techniques based on solving the fully viscous Navier-Stokes equations have been extensively applied to ship hydrodynamics with fruitful results, as they consider the important features of the actual flow, such as viscous effects and turbulence. Hence, they are more reliable for predicting ship's resistance and motions. (Stern, 2013) summarised the achievements made regarding ship hydrodynamics using CFD in the last decade. Further, recent progress in modern computational ship hydrodynamics with respect to shallow and confined water has been made. (Elloot et al., 2015) performed a turning circle and a zigzag test on a KVLCC2 hull model to determine the manoeuvring performance in a shallow water zone. To study the scale effect, (Tezdogan et al., 2016) performed unsteady Reynolds-averaged Navier-Stokes (RANS) simulations at full-scale for the squat in shallow water with STAR-CCM+ commercial software. They compared the results to the 3D potential flow theory and the experimental data of Mucha et al. (2014). They reported an underestimation of the ship squat and pointed indicated that the ship's resistance is sensitive to sinkage. (Linde et al., 2016) validated this observation with FLUENT, by simulating the ship's resistance both with and without consideration of ship sinkage. The predicted value of resistance with sinkage was closer to the experimental data. (Kaidi et al.,

2017) further studied the ship manoeuvring with FLUENT under the effect of bank-propeller hull interaction in shallow water.

In ports, flow stratification might occur as the non-saline, light river water flows into the colder and heavier saline seawater, leading to large horizontal or vertical fluid density variations. Highly density-stratified waters are known to pose particular challenges to navigating ships. When a ship's keel (bottom) is travelling just above the interface of the water layers, the ship experiences large wave resistance. This resistance occurs particularly if the ship is travelling close to the speed of the fastest internal waves, due to the generation of large internal waves. This phenomenon, known as 'dead water', affects the ability of ships to move through stratified water. Accurately assessing the effects of stratified flow on ship navigation requires a detailed knowledge of the flow field, including turbulent mixing and in particular, the generation of internal waves on the interface between the two layers of water.

Crapper (1967) and Hudimac (1961) presented analytical approaches to study the internal wave modes caused by a moving body in a two-layered ocean. It follows from their work that—just as for surface waves—at ship speeds sufficiently larger than the internal wave speed, only divergent waves travel downstream from the ship, while both divergent and transverse waves are present for slower ships. (Tulin et al., 2000) suggested a nonlinear theory to capture internal wave behaviour at high Froude number (Fn) in weakly stratified flow, which compared satisfactorily with available experimental results for a semi-submerged spheroid. (Delefortrie et al., 2004; Delefortrie and Vantorre, 2005) conducted a large number of experiments on towing tanks. They studied the mud layer effect on the ship manoeuvring by considering several parameters. They also developed a mathematical model to take into account the mud effect. (Chang et al., 2006) presented one of the few available examples of the use of CFD for a ship in a stratified medium. (Esmaeilpour et al., 2016) studied the evolution of the stratified flow in the near field of a surface ship in detail. They demonstrated that the generation of internal waves requires energy, which results in an increase in resistance.

In this paper, we present an overview of a numerical study of the mud layer effect on ship's resistance and sinkage by using a multi-phased CFD method. Note that, the mud is supposed stratified, hence, the water and the mud were modelled as separate layers with average values of density and viscosity. The main objective of this work is to test the ability of the CFD method to simulate and assess the influence of the mud on the hydrodynamic forces acting on the ship's hull. Four parameters were tested: the mud properties, the ship speed (V_s), the mud thickness and the UKC. A preliminary study was conducted to first show the influence of the non-Newtonian behaviour of mud on the ship's resistance, and the

internal waves at the mud-water interface. Based on this preliminary study, the Newtonian model was selected for this investigation. The UKC level was referenced to the water-mud interface; hence, it can take both positive and negative values. The limits of the CFD method are discussed in Section 5.

2 MATHEMATICAL FORMULATION AND NUMERICAL METHODS

The fluid flow is governed by the incompressible viscous Navier-Stokes equations completed with the continuity equation, as follows:

$$\nabla \cdot \mathbf{u} = 0 \quad (1)$$

$$\frac{\partial \mathbf{u}}{\partial t} + \nabla \cdot (\mathbf{u} \otimes \mathbf{u}) = -\frac{1}{\rho} \nabla p + \frac{\eta}{\rho} \nabla^2 \mathbf{u} \quad (2)$$

where \mathbf{u} and p represent the velocity vector and pressure, respectively, and ρ and η are the fluid properties of density and kinematic viscosity.

2.1 TURBULENCE MODELLING

To model the turbulence effect, the Reynolds averaging was computed on the flow variable in time, which gave rise to

$$\nabla \cdot \mathbf{U} = 0 \quad (3)$$

$$\frac{\partial \mathbf{U}}{\partial t} + \nabla \cdot (\mathbf{U} \otimes \mathbf{U}) = -\frac{1}{\rho} \nabla p + \frac{\eta}{\rho} \nabla^2 \mathbf{U} - \nabla \cdot (\mathbf{u}' \otimes \mathbf{u}') \quad (4)$$

where $\mathbf{u} = \mathbf{U} + \mathbf{u}'$ and $p = P + p'$. The last term in the RANS momentum equation is the Reynolds stress, which is often approximated by turbulence models. In this research, we employed the *SST k- ω* turbulence model, which is actually a combination of the *k- ω* and *k- ϵ* models while a shifting function is used to switch one from another.

2.2 MULTIPHASE APPROACH

The volume of fluid (VoF) method was used to simulate three-phase interactions (the interface of air/water and water/mud). Using this approach, both interfaces can be captured in a fixed grid by solving the continuity equation of the volume fraction (Eq. 5), as follows:

$$\frac{\partial \alpha_p}{\partial t} + \mathbf{u} \nabla \alpha_p = 0 \quad (p = 1, 2) \quad (5)$$

α_p denotes the volume fraction of the p^{th} fluid, and:

$$\sum_{p=1}^n \alpha_p = 1 \quad (n = 2 \text{ or } 3) \quad (6)$$

Equations presented thus far (Eq. 1–6) are solved using the commercial code Ansys-Fluent 13.0 based on the finite volume method. The pressure-velocity coupling was ensured by using a steady pressure-based coupled algorithm, and the interpolation method selected to compute the cell-face pressure was the PREssure STaggering Option (PRESTO). The second order was set for the VoF's special discretisation.

2.3 NON-NEWTONIAN BEHAVIOUR LAW FOR MUD

It should be noted that mud behaviour is often considered non-Newtonian, which means the viscosity depends on the shear rate. Hence, the Herschel-Bulkley model was selected to reproduce this behaviour. The Herschel-Bulkley model is represented by the following equations:

$$\tau = \tau_0 + K \dot{\gamma}^n \quad \text{if } \tau > \tau_0 \quad (7)$$

$$\tau = 0 \quad \text{if } \tau \leq \tau_0 \quad (8)$$

where, τ and τ_0 are shear and yield stress, respectively. K is the consistency factor, n is the power law exponent, and $\dot{\gamma}$ is the shear rate.

The non-Newtonian viscosity η is computed using one of the following formulas:

$$\eta = \frac{\tau_0}{\dot{\gamma}} + K \dot{\gamma}^{n-1} \quad \text{for } \dot{\gamma} > \dot{\gamma}_c \quad (9)$$

$$\eta = \frac{\tau_0 \left(2 - \frac{\dot{\gamma}}{\dot{\gamma}_c} \right)}{\dot{\gamma}} + K \dot{\gamma}_c^{n-1} \left[(2 - n) + (n - 1) \frac{\dot{\gamma}}{\dot{\gamma}_c} \right] \quad \text{for } \dot{\gamma} < \dot{\gamma}_c \quad (10)$$

$\dot{\gamma}_c$ is the critical shear rate.

Figure 3 shows the variation of the shear stress with shear rate according to the Herschel-Bulkley model.

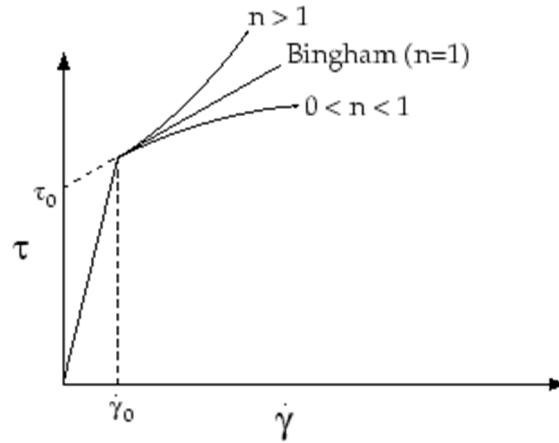


Figure 3. Shear stress as a function of the shear rate basing on the Herschel-Bulkley model (This figure was taken from the Fluent software manual)

2.4 VERIFICATION AND VALIDATION OF THE CFD MODEL

The procedures for verification and validation of the CFD model have been discussed and performed in several previous works (Kaidi et al., 2017, 2018; Razgallah et al., 2018; Ali et al., 2018), and were carried out in accordance with the ITTC recommendations. Verification consisted of tests and analysis of the results of several mesh qualities, whilst validation was performed by taking the numerical results of the ship's resistance, the profile of generated waves, and the ship's squat and comparing them to the measurements carried out in a towing tank of the University of Liège and the Central School of Nantes. Note that no mud layer was considered in these works: only the water-air interface was modelled and validated.

Based on the obtained results, it was concluded that the CFD model provided a good estimate of the hydrodynamic forces around the ship's hull, and correctly captured the air-water interface. It was also concluded that the CFD model could simulate the sediment suspension and transport accurately (Kaidi et al., 2018).

3 STUDIED SHIP, CHANNEL CONFIGURATION, BOUNDARY CONDITIONS, AND MUD PROPERTIES

To conduct this investigation, we used a container cargo-hull form (see Figure 4). This kind of ship was selected because it is one of the most common ships to sail in the Gironde estuary. Table 1 provides the main characteristics of the hull, where, L_{PP} is the length between perpendicular, L_{OA} is the length over all, B is the ship beam, T is the ship draft, and C_B is the block coefficient. Note that the same reference frame is used in this investigation. The origin of this reference is

fixed on the ship, where the $x = 0$ corresponds to the ship's bow plane, while, the $z = 0$ corresponds to the ship's keel plane. The X-axis is oriented right while the Z-axis is oriented up as is shown in Figure 4.

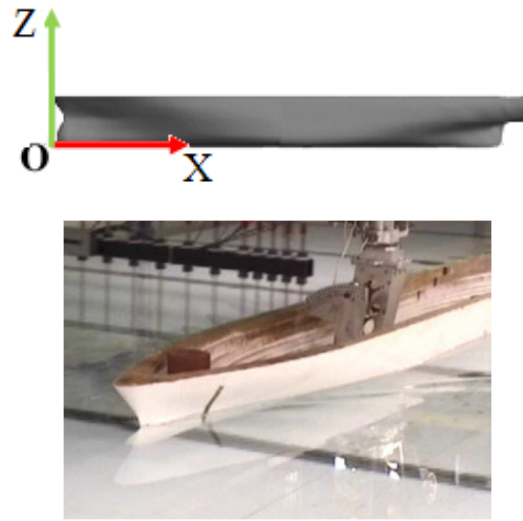


Figure 4. Container carrier-hull form.

Table 1. Ship dimensions and scales

| Ship | Container cargo | |
|--------------|-----------------|-------|
| Scale | 1/1 | 1/80 |
| L_{PP} (m) | 230.0 | 2.875 |
| L_{OA} (m) | 232.5 | 2.906 |
| B (m) | 32.2 | 0.402 |
| T (m) | 10.0 | 0.125 |
| C_B | 0.681 | 0.681 |

In the present study, we considered only the confinement effect using the UKC. To prevent large body motions, the reference frame was fixed on the ship; hence, the fluid and other parts moved relative to the hull. The computational domain was chosen with a rectangular section, large enough such that there was little influence of the position of the inlet and outlet: 1–2 L_{pp} for the inlet and 3–5 L_{pp} for the outlet are recommended by ITTC (ITTC, 2011). Half of the computational domain was used to reduce computational time.

For the boundary conditions, at the inlet the flow velocity was imposed, and at the outlet the outflow condition was used. A symmetrical condition was applied at the top, at the mid-plane, and at the side boundaries. At atmosphere, total pres-

sure was applied; at the bottom moving wall condition was employed to take into account the relative motion, and at the hull's surface no-slip wall condition was used.

Four combinations of mud properties were selected to conduct this investigation. These properties represent the average values measured at different zones in the Gironde estuary and some ports. Table 2 presents the combination of the density and viscosity of the mud.

Table 2. Physical properties of tested mud

| Mud type | density (kg/m ³) | viscosity (Pa.s) |
|----------|------------------------------|------------------|
| Mud A | 1085 | 0.025 |
| Mud B | 1160 | 0.068 |
| Mud C | 1210 | 0.128 |
| Mud D | 1230 | 0.260 |

4 RESULTS AND DISCUSSION

4.1 COMPARISON BETWEEN THE NEWTONIAN AND NON-NEWTONIAN MODELS

The effect of the use of non-Newtonian viscosity to simulate the mud behaviour is discussed in this section. Using the CFD method, the mud layer could be modelled in different ways. The first was to suppose that the mud properties were constant and slightly influenced by the shear stress induced by the ship's passage. Hence, we used average values for the density and the viscosity. The second was to consider that the mud was significantly affected by the shear stress, from where a non-Newtonian model was used to estimate the dynamic viscosity.

It should be highlighted that in the estuary environment, the flow was modelled using hydraulic models, which estimate the average turbulent viscosity at the channel bottom that can be used by manoeuvring simulators. This provides indispensable results for assessing the difference between the results obtained by both approaches.

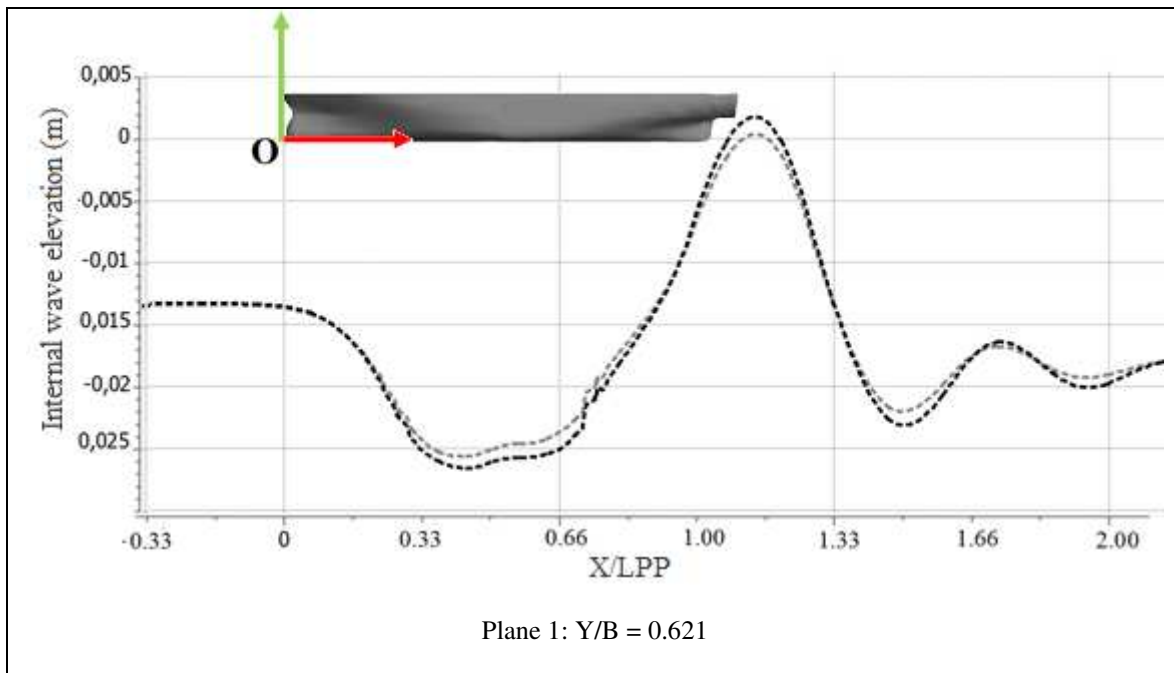
To carry out this study, the ship's draft was set to 10 m (0.125 m in the model) and the ship's speed was set to 10 kn (0.575 m/s). The mud thickness used was 3 m in full scale (0.0375 m in the scaled model), which corresponds to the

250 average thickness in the estuaries. The UKC value was set to $+10\% \cdot T$ with respect to the mud/water interface, which
 251 corresponded in our case to 1 m in full scale (0.0125 m in the scaled model).

252

253 Figures 5 and 6 present a comparison between the undulations of the mud/water interface obtained using both methods
 254 for mud types A and C at two different plans (see Figure 7). The first plane is located at Y/B of 0.621 while the second is
 255 located at $Y/B = 1.243$, where Y is the lateral distance from the ship's mid-plan and B is the ship's beam. The x-axis of
 256 these figures represented the dimensionless distance X/LPP , where X is the longitudinal distance from the ship's bow
 257 and LPP is the length of the ship, and the z-axis represented the undulation elevation. Generally, we remark that the non-
 258 Newtonian model tends to underestimate the mud layer crests. As is evident, the difference between both models shows
 259 that mud A has a smaller viscosity and density compared to mud C. The height difference at the crest and trough is al-
 260 most similar; approximately 11% at plane 1 and 18% at plane 2 for mud A, and approximately 16% at plane 1 and 30%
 261 at plane 2 for mud C. The difference is larger at plane 2, because, the area affected by the ship's passage is reduced
 262 when the mud is considered non-Newtonian, especially at high density and viscosity, as shown in Figure 7.

263



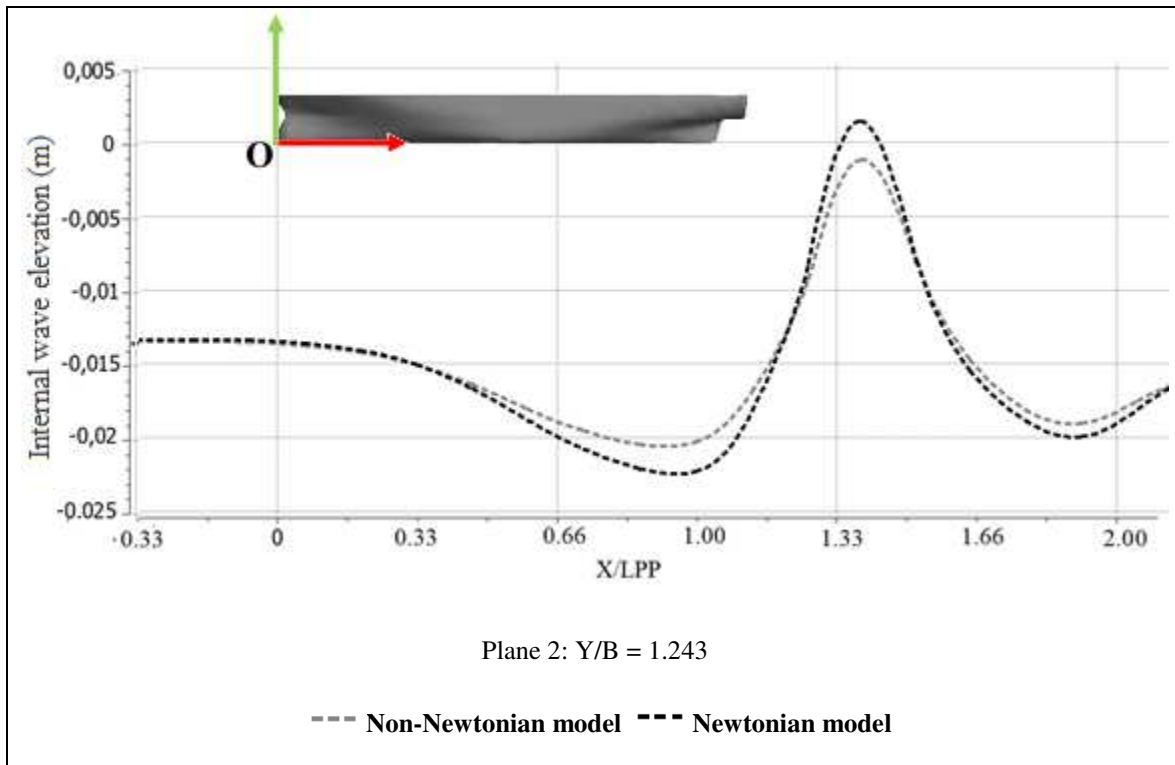
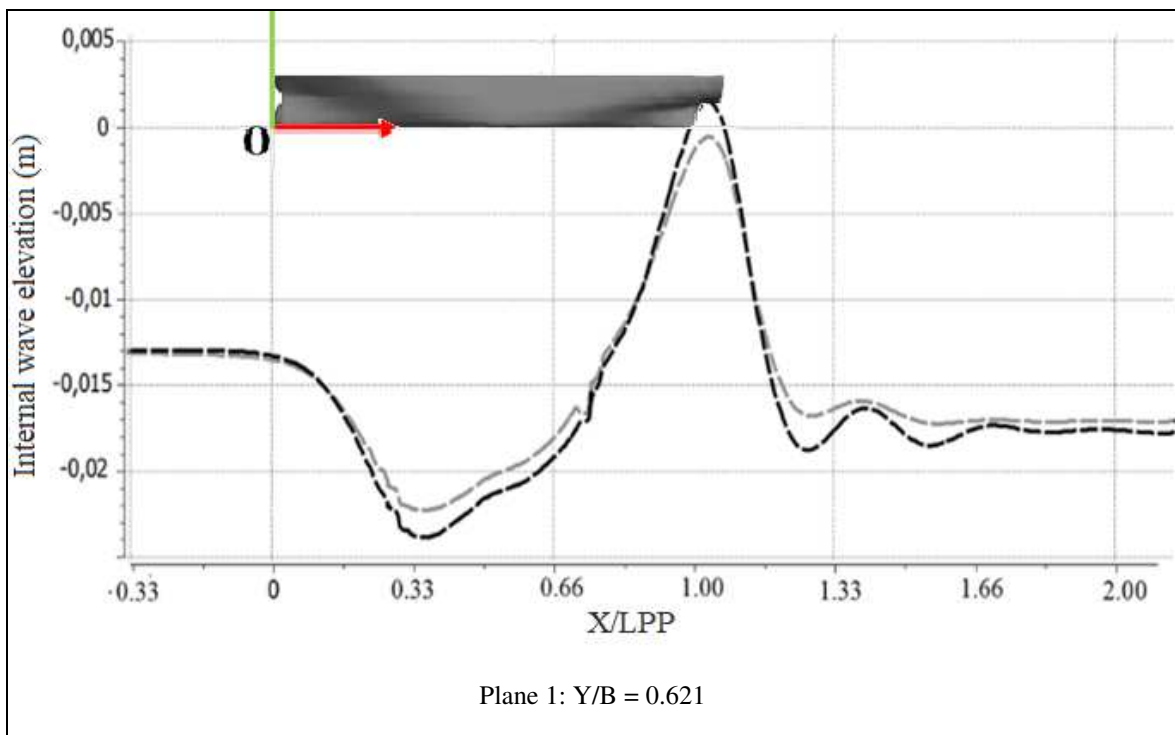


Figure 5. Undulation of mud A at two different planes from the mid ship.



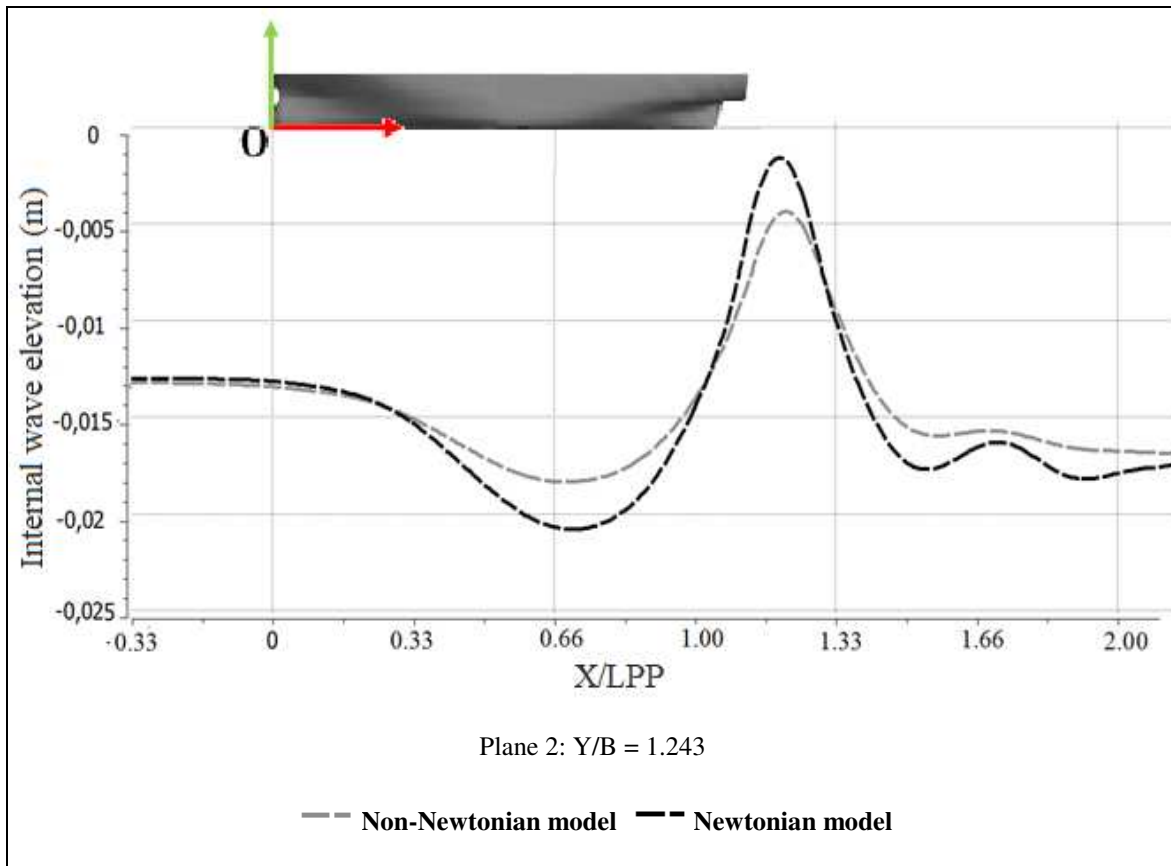


Figure 6. Undulation of mud C at two different planes from the mid ship.

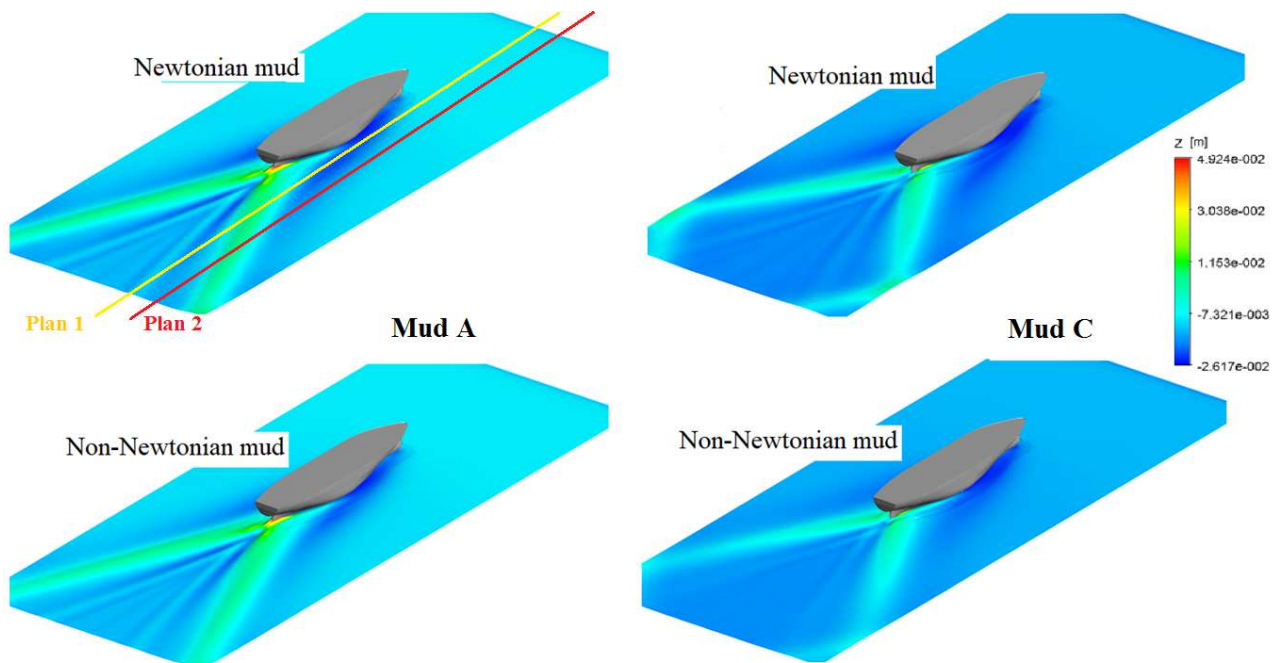


Figure 7. Iso-surface of internal waves for mud A and C by considering a Newtonian and non-Newtonian model (UKC = +10%).

To assess the ship's resistance, two UKCs were tested (+10% and -10%). For the two types of mud, the difference between the Newtonian and non-Newtonian models was small, as presented in Table 3 (approximately 2% for both mud A and mud C at positive UKC, and less than 5% at negative UKC. Note that, the verification and validation procedure shows that the uncertainty of the total resistance was about 7% in very confined water. This uncertainty corresponds to a monotonic convergence condition with an order of accuracy of 1.86. Based on these values, the only conclusion that can be drawn from this comparative analysis is that the Newtonian model gives an acceptable estimation of the ship's resistance despite the overestimation of the mud/water undulation. Hence, the Newtonian model can be used to carry out this investigation.

Table 3. Computed ship's resistance (half of ship) using the Newtonian and non-Newtonian models.

| Ship's resistance | | | Δ |
|-------------------|---------------|----------------|----------|
| | Newtonian | Non- Newtonian | |
| UKC = +10% | | | |
| Mud A | 1.125±0.078 N | 1.149±0.080 N | 2.08% |
| Mud C | 1.328±0.093 N | 1.356±0.095 N | 2.06% |
| UKC = -10% | | | |
| Mud A | 2.302±0.160 N | 2.415±0.170 N | 4.76% |
| Mud C | 2.652±0.185 N | 2.623±0.182 N | 1.10% |

4.2 INFLUENCE OF MUD PROPERTIES ON SEABED UNDULATION AND FREE SURFACE ATTENUATION

Here, the mud layer thickness was set to 3 m (0.0375 m in the scaled model). The ship's draft and speed were set to 10 m (0.125 m in the scaled model) and 10 kn (0.575 m/s in the scaled model), respectively. The value chosen for the UKC with respect to the mud/water interface was +10%*T.

Figure 8 illustrates the profile of the mud layer deformation caused by the ship's passage. As can be seen, the deformation is composed of a principal undulation and secondary undulations. The principal undulation is similar to the free surface deformation with a small shift, where a stern divergent wave is observed (Figure 9). The divergence angle, the wave height, and the wavelength of this wave depend on the mud properties, as shown in Figure 10. In this study, we only focused on the principal undulation, which had an impact on the ship manoeuvring, principally on the ship's re-

sistance and squat. This undulation was characterised by a maximum trough and crest, where generally the trough is located at the mid hull, whilst the crest is located at the hull's stern. For all tested mud properties, the mud layer trough started from the same position (the ship's bow). However, compared to the initial mud setup, the trough level and length increased by decreasing the mud viscosity. We note that the origin of this trough was principally the pressure variation along the ship hull caused by the return flow, which was influenced by the mud properties (see Figure 11). From the same figure, it can be seen that the relative increase of the mud trough shows a linear variation for viscosities varying between 0.025 and 0.12 Pa.s.

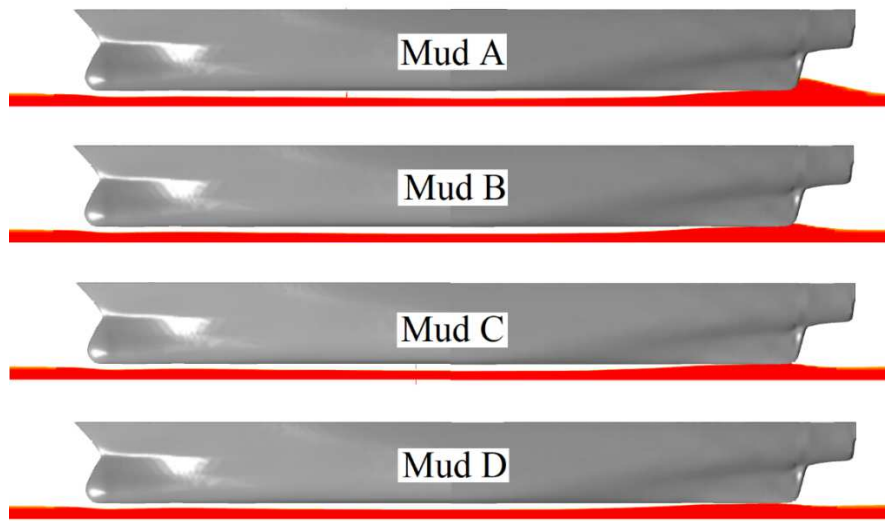


Figure 8. Profile of the mud layer undulation at the ship symmetry plane.

It can also be observed that the physical properties of the mud played an important role on the mud crest, the location of this crest, and in some situations the hull/mud contact area. When the density and viscosity of the mud were smaller, the mud was considered more fluid; hence, the later behaved as a denser fluid and followed the water flow. When the viscosity of the mud was greater, the mud layer was more solid and its behaviour was more rigid. From this, we noted a maximum uprising value for the mud D ~20% less than for mud B, whilst an insignificant variation was noted between mud samples B and A.

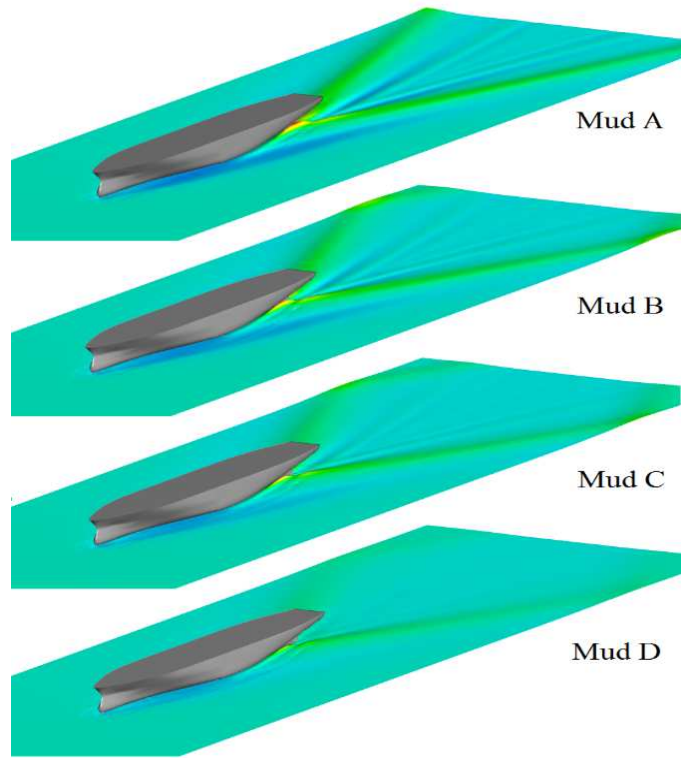


Figure 9. Iso-surface of the internal waves as a function of mud properties.

For all tested properties, the mud uprising position varied as the mud properties varied. From simulated cases, it was noted that the lower the viscosity, the more the mud uprising moved backwards. The same observations were also noted by Delefortrie and Vantorre (2005). Contact between the hull and the mud was also observed for mud A and B and the contact area was slightly larger in the case of mud A.

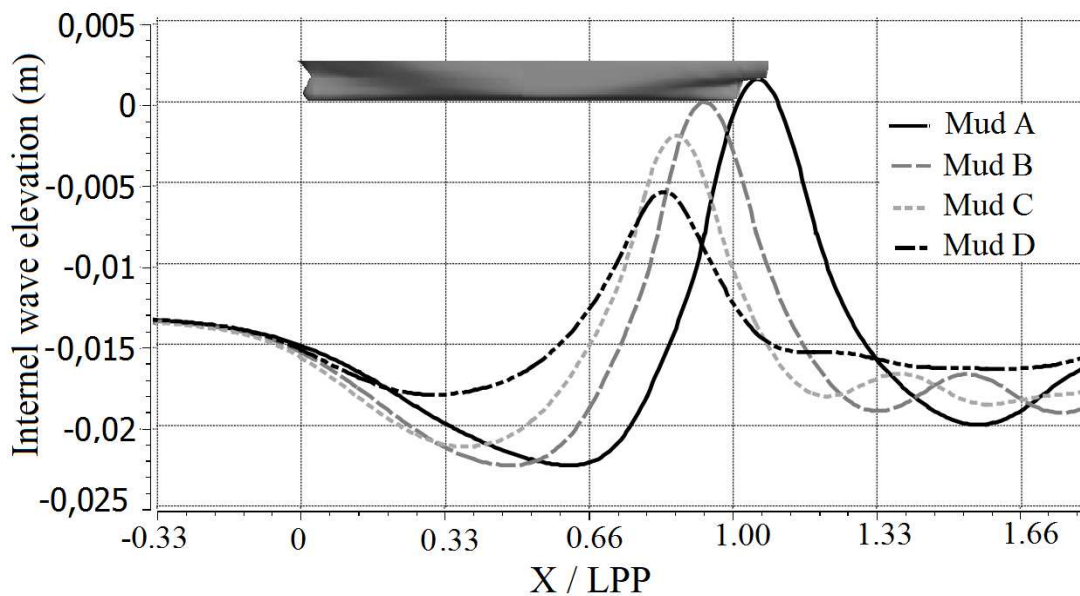


Figure 10. Mud layer undulation along the channel as a function of mud properties (cut at ship's mid-plan).

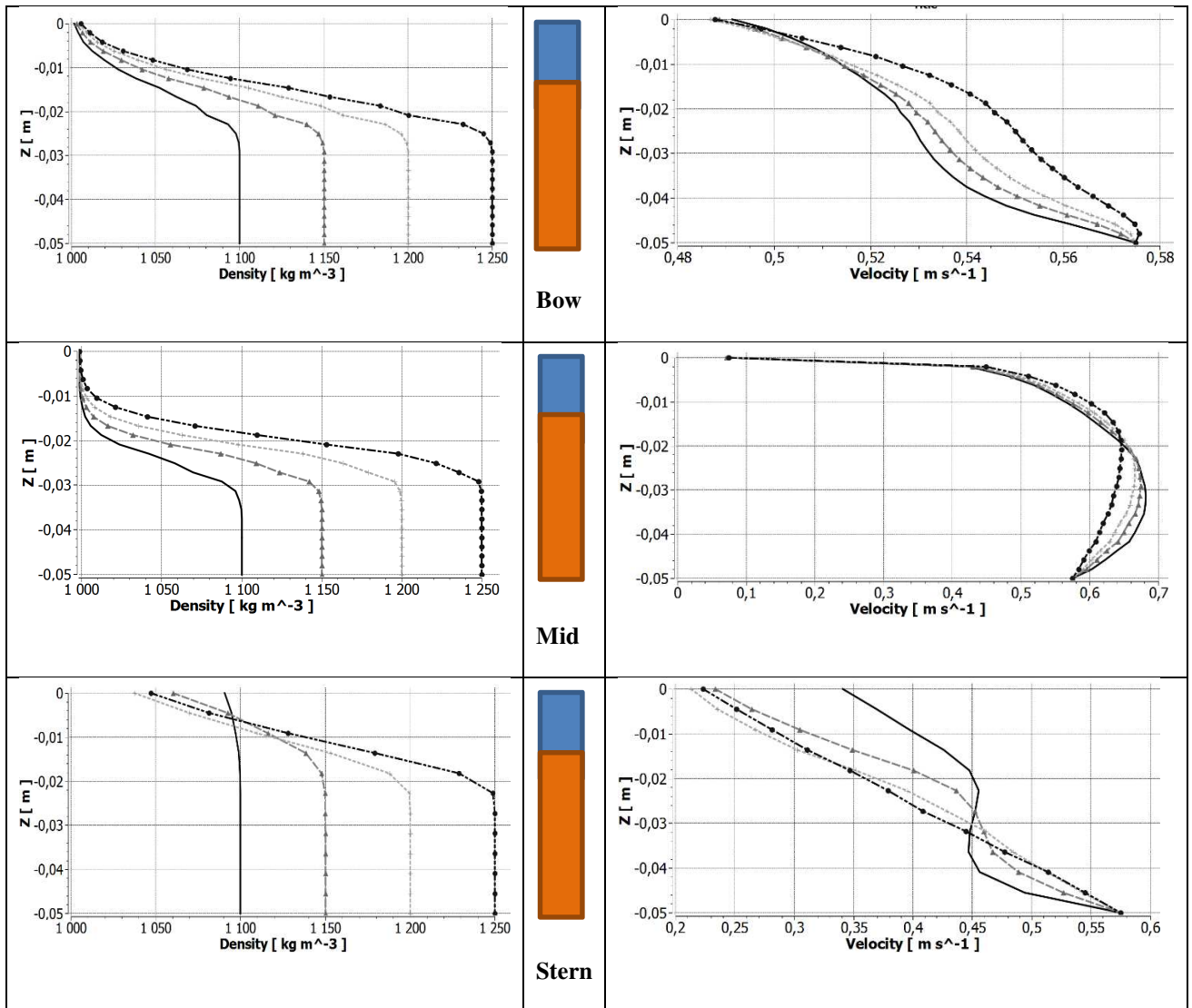


Figure 11. Vertical profile of density and flow velocity under the ship at bow, mid, and stern of the ship.

To assess the separate effect of the viscosity and the density on the internal waves pattern, an additional series of simulations were performed. For a better visibility of this undulation, the mud thickness of 3 m in full scale was used (1 m corresponds to the UKC and 2 m to the distance between the ship's keel and the solid seabed) for a negative UKC of -10%*T. Five values of viscosity and density were tested. The ship's speed was set to 10 kn as in the previous simulations. First, the viscosity was varied as follows: 0.005, 0.01, 0.05, 0.1, 0.2 Pa.s, while the density of the mud was set to 1100 kg/m³, and second, the viscosity of the mud was set to 0.1 Pa.s which corresponds approximately to the transition limit defined by Delefortrie (2016) basing on experiments. While the density was varied as following: 1050, 1100, 1150, 1200 and 1250 kg/m³.

The internal waves corresponding to the viscosity and the density variation were plotted in Figure 12. As it can be seen at the left of this figure, the viscosity has a very important influence on the internal waves pattern, and for the used ship's speed the internal bow waves length is longer than the ship's length which is a characteristic of shallow water navigation. For the smallest viscosity, a stern waves pattern was observed, where the first is convergent, while the second is divergent which resembles to the free surface behaviour in a shallow water. Reflected waves were also observed far behind the ship's stern. By increasing the viscosity value to 0.01 Pa.s, the same waves pattern were observed, however, transverses waves appeared behind the ship's stern. For viscosity value of 0.05 Pa.s, the waves pattern becomes more apparent, while the angle of the diverging waves increases and tends to be perpendicular to the ship's heading direction. The same observations were noted for the viscosity value of 0.1 Pa.s, The converging waves remains unchanged and apparent, whereas the diverging waves becomes completely transversal and slightly less apparent. For the highest mud viscosity (0.2 Pa.s), only the transverses waves pattern were affected and becomes even less apparent and tend to disappear. This behaviour, is in accordance with experimental findings, however, viscosity limits defining waves patterns were slightly different.

The density variation effect on the internal waves pattern is shown at the right of Figure 12. The only observation noted from this figure is that the density has any effect on the transverses waves, while the converging waves increase slowly by increasing the mud density.

Basing on these results it can be concluded that the internal Froude number Fn_i ($Fn_i = Fn \sqrt{(\rho_w + \rho_m)/\Delta\rho}$) often used to describe multiphasic flow cannot be used to define the internal waves patterns. It can also be concluded, that the internal waves pattern evolution should be set as a function of mud viscosity and mud layer thickness.

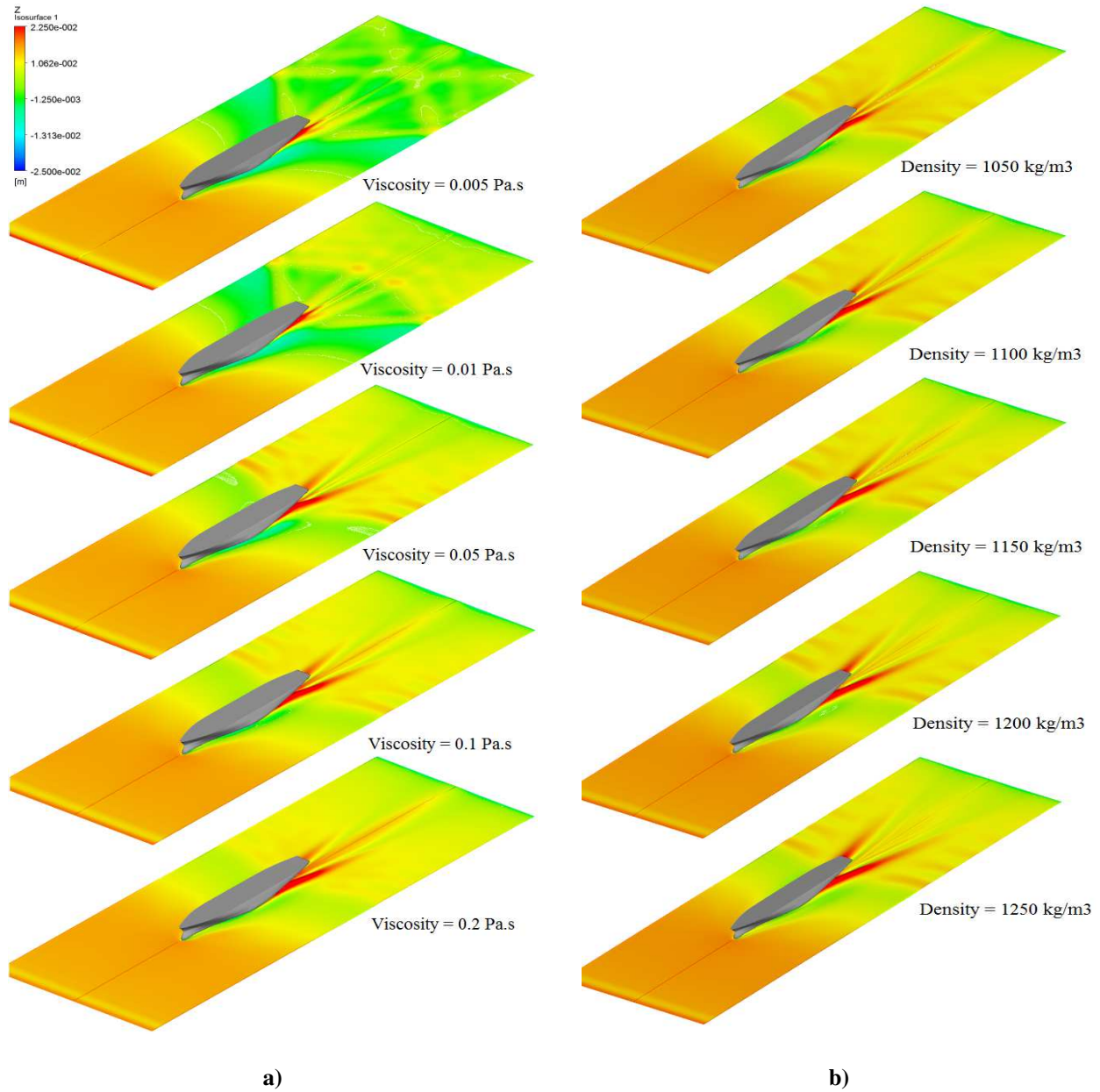


Figure 12. Internal waves: a) viscosity variation and b) density variation

Figure 13 shows the free surface attenuation caused by the mud layer. For this, we compared the free surface deformation of a channel (with a muddy layer) to the free surface deformation of a channel without a muddy layer (rigid bottom). The same total depth was maintained for both tests. Note that for the present study, the total depth of the channel is the sum of the ship's draft, the UKC, and the mud thickness. It may be observed that the free surface elevations closely resemble the mud layer undulation. It was also observed that the trough and crest of the free surface was approximately the same between the rigid seabed and mud samples A, B, and C. However, for mud D, we noted a lowering of the free surface. This lowering was essentially caused by the effect of shallow water. As mentioned above, the higher the viscosity, the more solid the mud; hence, the seabed can be considered solid. The shear stress due to the high viscosity of the

mud slowed down the flow velocity of the mud/water interface under the ship's hull, inducing an acceleration of the water flow and consequently a pressure drop.

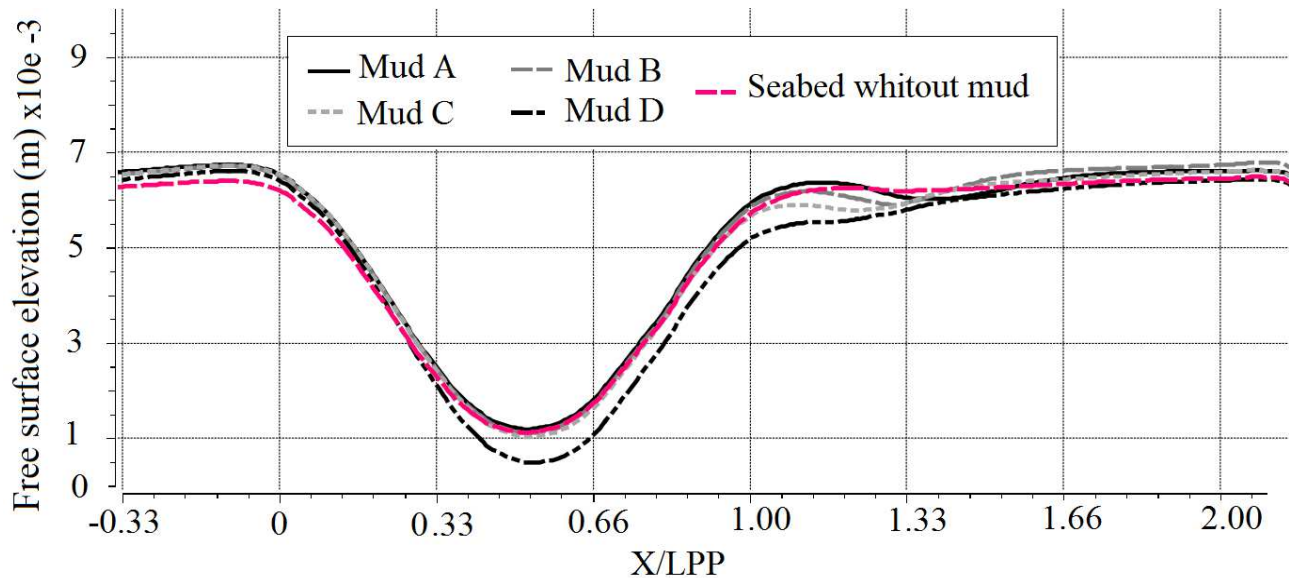


Figure 13. Comparison between the free surface elevation of seabed with and without the muddy layer.

4.3 SHIP'S SPEED AND MUD THICKNESS EFFECT ON THE SEABED UNDULATION (INTERNAL WAVES PATTERN)

The study of the influence of the ship's speed and the mud's thickness on the seabed undulation is presented in this section. The influence of the ship's speed was performed by setting the mud layer thickness to 3 m in full scale, and the UKC to $+10\% \cdot T$. Mud A was selected for this simulation. The ship speeds that were tested were 6, 8, and 10 kn in full scale (0.345, 0.46, and 0.575 m/s in the scaled model). It can be seen from Figure 14 that for the selected mud, the ship's speed has an influence on the position of the maximum rise of the undulation. The higher the speed, the more the undulation crest moved backwards. It was also seen that the crest width increased as the ship's speed increased. This behaviour was due first to the mud type. Here, the mud density was small and it was thus more fluid than solid. Second, the return current amplification caused by the increase in the ship's speed affected the behaviour. A slight influence of the ship's speed on the trough depth and the crest height of the mud/water interface undulation was noted.

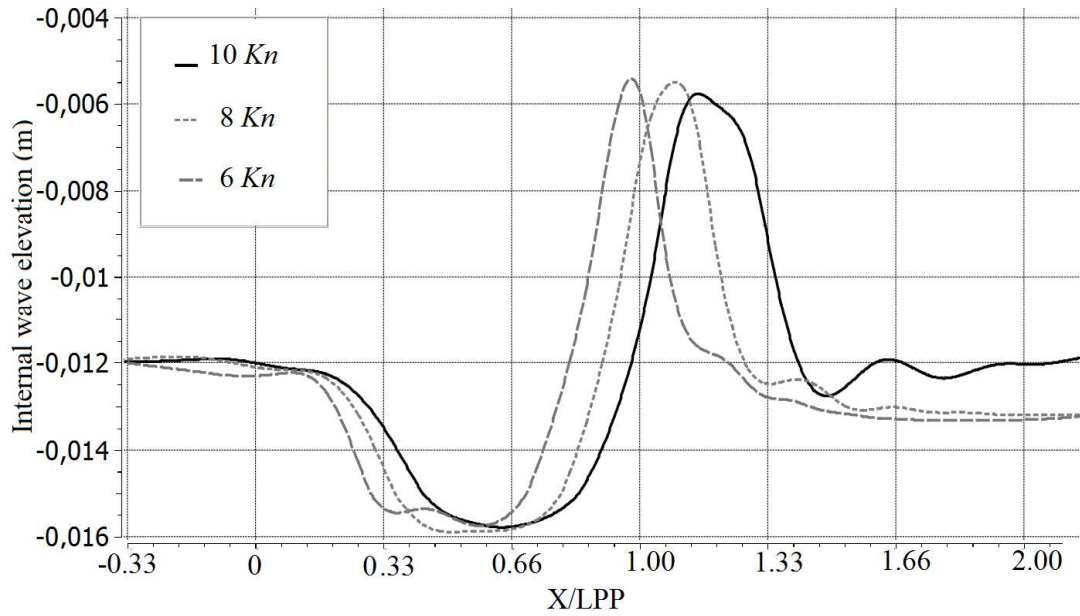
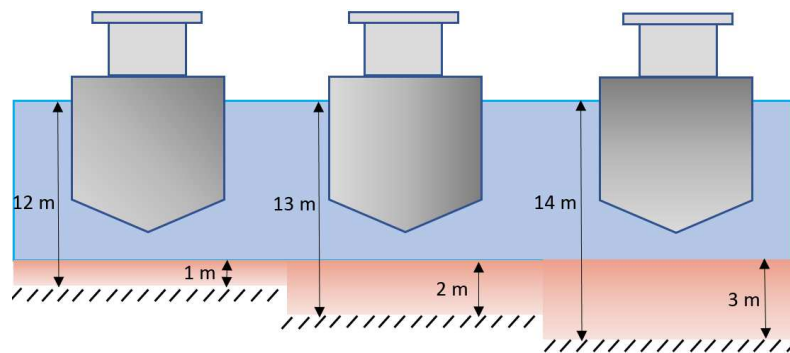
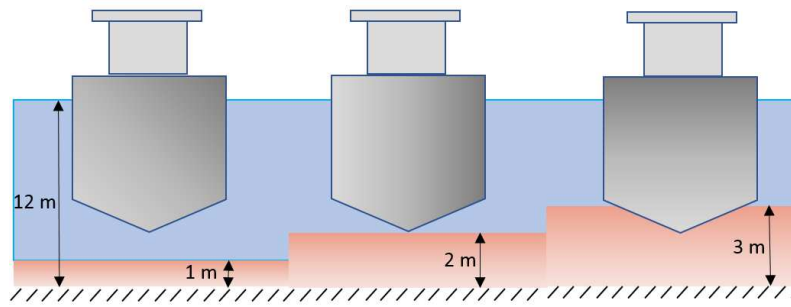


Figure 14. Mud layer undulation along the channel as a function of the ship speed (cut at the ship's mid-plan). X is the longitudinal position.

In the second part of this section the influence of the mud thickness on the internal waves pattern was studied. Three thicknesses of the mud A were tested: 1 m, 2 m and 3 m in full scale. Note that the mud thickness effect on the internal waves patterns can be tested using a constant UKC ($10\% \cdot T$) and variable total depth as is depicted in Figure 15-a or using a variable UKC ($+10\% \cdot T$, $0\% \cdot T$ and $-10\% \cdot T$) and constant total depth as is depicted in Figure 15-b. The ship's speed was set to 10 kn (0.575 m/s in the scaled model). The Fr_h values were the same for both type of test 1.64, 1.16 and 0.94 (using the mud thickness as a characteristic length) for mud thickness of 1m, 2m and 3m respectively. These values correspond to critical and supercritical regimes. The numerical results of the waves patterns were shown in Figure 16.



(a)



(b)

Figure 15. Mud thickness variation: (a) variable total depth and (b) constant total depth.

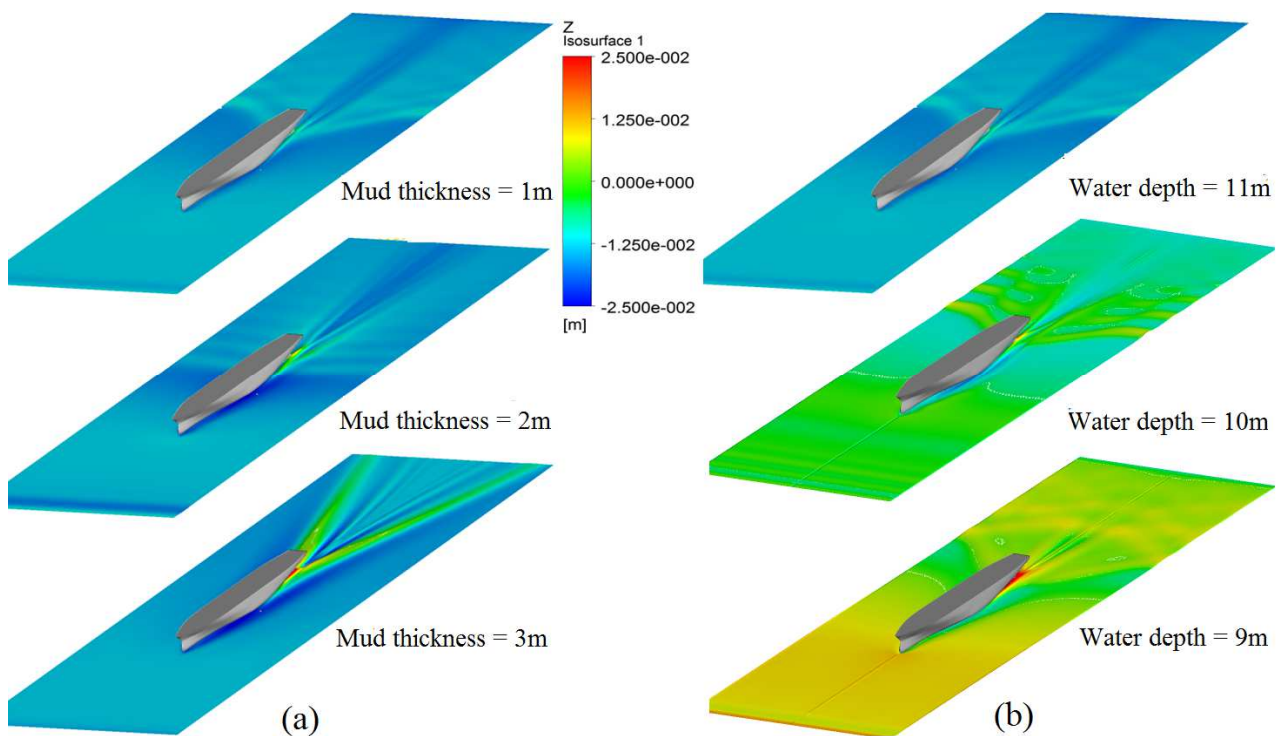


Figure 16. Internal waves patterns as a function of mud thickness : (a) constant UKC and variable total depth and (b) variable UKC and constant total depth.

Figure 16-a shows the influence of the mud thickness on the internal waves patterns for a constant UKC and variable total depth. From this figure it can be shown three different waves patterns of the seabed. Where for the smaller mud thickness (1m in full scale), the internal waves appear behind the ship's stern and its pattern is very divergent and nearly transversal to the ship's heading direction. For the medium thickness (2 m in full scale), the undulation is principally transversal, however, a small Kelvin pattern appears at the ship's stern, which leads us to consider this thickness as a transition thickness. For the larger mud thickness (3m in full scale), the internal waves have a Kelvin pattern form. These patterns were also noted in the experimental work done by Delefortrie(2016) (see Figure 17). The authors of this

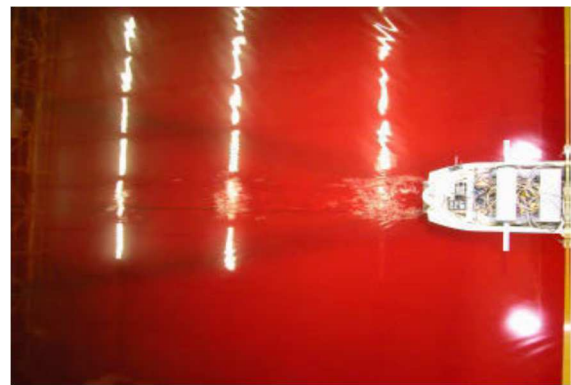
work related these patterns only to the mud viscosity and the ship's speed. According to their findings: the Kelvin pattern appeared for larger ship's speed and lower viscosities ($< 0.12 \text{ Pa.s}$), and the transversal pattern appeared in the case of lower ship's speed. It was also noted that the transversal pattern were observed for larger ship's speed and larger mud viscosities ($> 0.12 \text{ Pa.s}$). In the present work the both undulation patterns (transversal and Kelvin pattern) were observed by varying only the mud thickness. Where, the ship's speed can be considered larger, however, the mud viscosity is lower (0.025 Pa.s).

To separate the effect of the mud thickness and the effect of the confinement, the total depth was considered constant and the mud thickness was varied. The obtained results were depicted in Figure 16-b. The simulation setup for the smaller mud thickness (1m in full scale) is the same as in the case of variable total depth hence the results of the previous simulation were kept. For the medium mud thickness (2m in full scale) the UKC is $0\% \cdot T$, the similar waves pattern as for the mud thickness of 1m was observed, however, the undulation amplitude was amplified. For larger mud thickness (UKC = $-10\% \cdot T$) the waves change pattern where a convergence and divergence waves appear. Transversal waves were also observed far behind the ship. From these observations, it can be concluded that the mud thickness has a significant influence on the internal waves pattern which change as a function of the total depth and the UKC, however, it is difficult to specify exactly the influence of the mud thickness. In fact, the mud thickness effect is always coupled with another parameter, either the total depth or the UKC. From this study it can also be concluded that the internal waves pattern are independent of the Frh contrary to the generated waves pattern at the water – air interface.

Basing on the results obtained in this section the pattern of internal waves are not only depends on the mud viscosity and ship's speed as is given in the literature but by the combined effect of the viscosity, the ship's speed, the mud thickness, the water depth and the UKC.



a) $\eta = 0.002 \text{ Pa.s}$



b) $\eta = 0.030 \text{ Pa.s}$

Figure 17. Measured mud layer undulation carried out by Delefortrie (2016)

4.4 SHIP'S RESISTANCE VARIATION DUE TO MUD PROPERTIES, SHIP'S SPEED AND MUD THICKNESS

It is known that ship's resistance is greatly affected by channel configuration (such as confinement and restrictions). In shallow water, the ship's resistance increases significantly due to the accelerated water around the hull, as explained previously. The presence of the mud layer in turn affects the flow under the ship's hull, inducing a variation in the ship's resistance. The effect of the latter can be considerably amplified if the UKC is negative.

In this section, findings are presented from studying the impact of the mud layer, first by testing the mud properties effect for a given mud thickness (3 m in full scale). Hence, the four mud properties were tested for an UKC of $+10\%T$ with respect to the mud/water interface. The ship's speed was set to 10 kn (0.575 m/s). No squat was considered in these simulations.

Figure 18 shows the ship's resistance variation caused by variations in the mud properties. From this figure, it is evident that the ship's resistance increased with mud viscosity, although there was no contact between the hull and the mud with mud samples C and D. This leads us to conclude that this increase essentially concerns the frictional component of the resistance. In fact, when the mud is consolidated it seems as though the total depth of the water is reduced, which makes the navigation environment more confined, and consequently, the return current velocity increases.

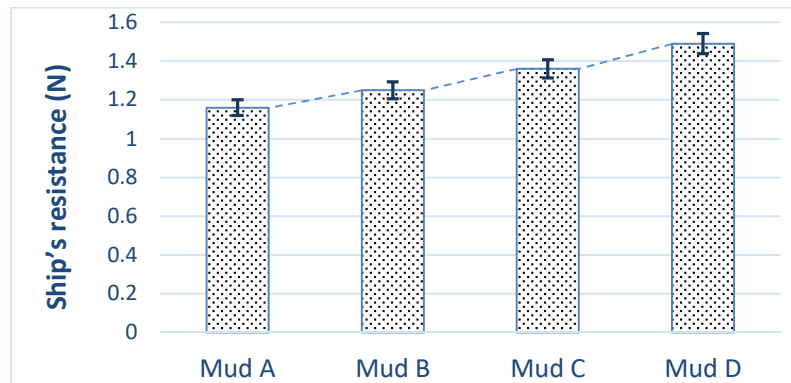


Figure 18. Ship's resistance (half of ship) as a function of mud properties (for a ship speed of 10 kn and UKC of $+10\%T$).

To understand better the confinement phenomenon due to the mud layer and its influence on the ship's resistance, we carried out simulations by varying the mud thickness. Three thicknesses were tested (1m, 2m and 3m in full scale). For each thickness we used two speeds (6 and 10 kn) and two types of mud (mud A and mud C). The water depth remains unchanged for all simulations (10 m in full scale). First, a positive UKC of $+10\%T$ was considered. The results of these simulations were shown in Figure 19.

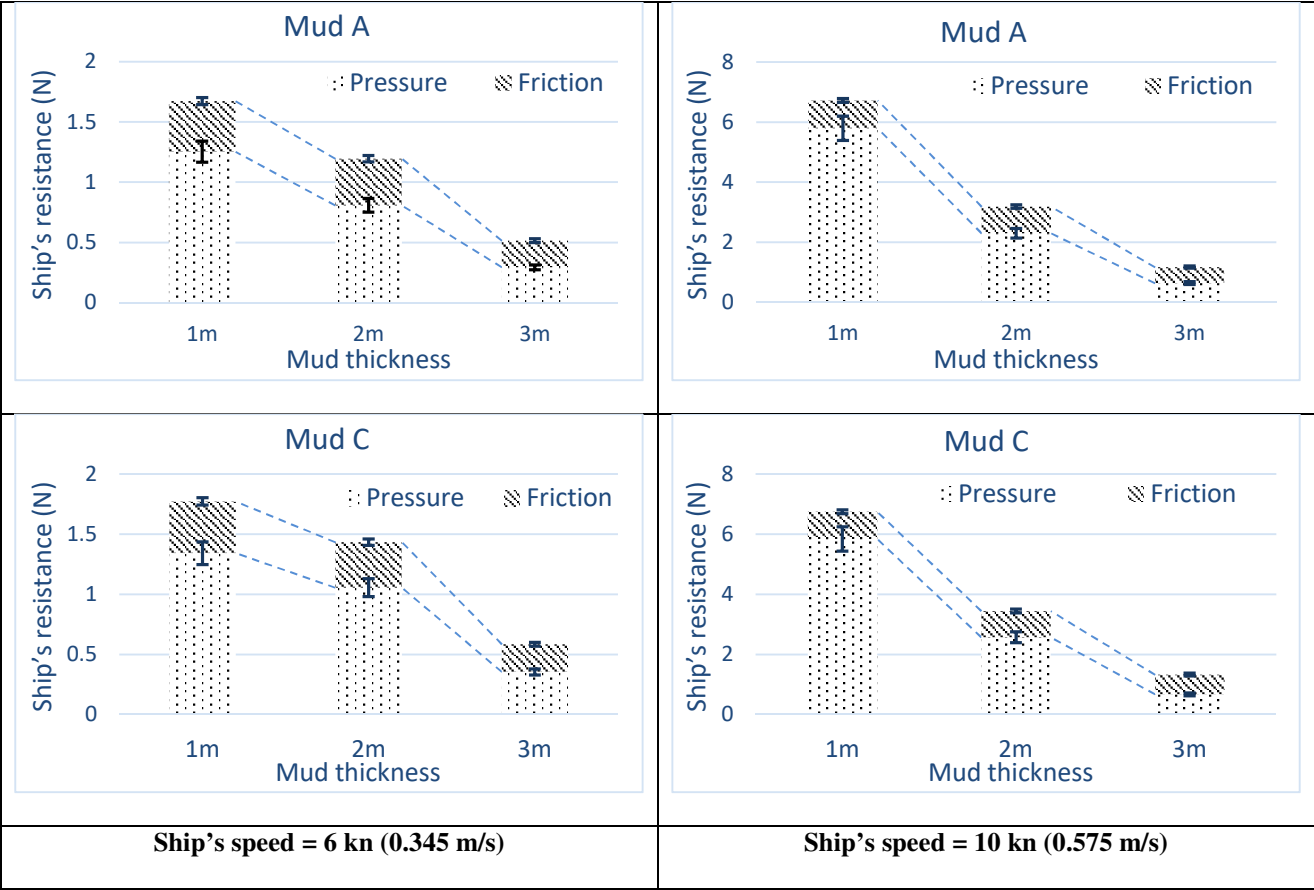


Figure 19. Ship's resistance (half of ship) variation as a function of mud thickness and ship's speed for mud A and mud C. UKC = +10%*T.

From these figures, it can be seen that the ship's resistance increases with increasing ship's speed. However, this increase is different according to the mud layer thickness as well as the type of the mud. In fact, by decreasing the mud layer thickness, the ship's resistance increases considerably. This increase concerns both types of forces: pressure and friction, however, the wave-making resistance remains the most dominant and the most impacted by this decrease in thickness.

The wave-making resistance is amplified about 9 times when the ship is sailing at a speed of 10 kn on a mud thickness of 1 m than 3 m, and about 4 times when the ship's speed is 6 kn. While the amplification of the friction resistance is of the order of 2 times for the two ship's speeds. It was also observed that the wave-making resistance was the most dominant compared to the friction resistance except in the case of the largest thickness (3 m), where both types of forces were approximately in the same range. This leads us to conclude that

Note that for navigation in channels with solid seabed the confinement is often defined by the ratio of water depth to ship's draft (hw/T). This ratio is an essential element for the calculation of the ship's resistance. In the case of navigation

in turbid water with a muddy bottom, this ratio may be valid however, the definition of the depth h_w must be modified by including the thickness of the mud layer. A proposal has already been made by Delefortrie (2016) proposing the use of the hydraulic depth (h^*) given by the following formula:

$$h^* = h_w + \phi h_m \quad (11)$$

Where, ϕ is the fluidization parameter which represents the mud type. So far, all works studying the influence of the mud quality on the ship's resistance were performed by varying both values of viscosity and density. In order to distinguish the influence of each physical property we varied separately the viscosity and the density of the mud. The same process as in the sub-section 4.3 was used: first, the density is fixed at 1100 kg / m and the viscosity is varied, then the viscosity is fixed at 0.1 Pa.s and the density is varied. For a better presentation of the influence of these properties on the ship's resistance, we considered the highest speed of navigation (10 kn) and assume that the ship's UKC is $-10\% * T$. Three mud layer thicknesses were tested (2 m, 3 m and 4 m) corresponding to a distance between the ship's keel and the solid seabed of 1 m, 2 m and 3 m as is presented in Figure 20.

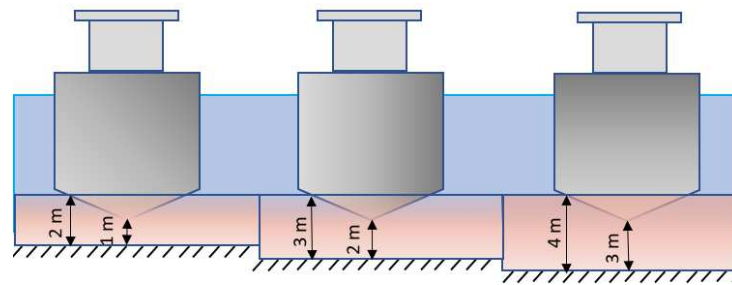
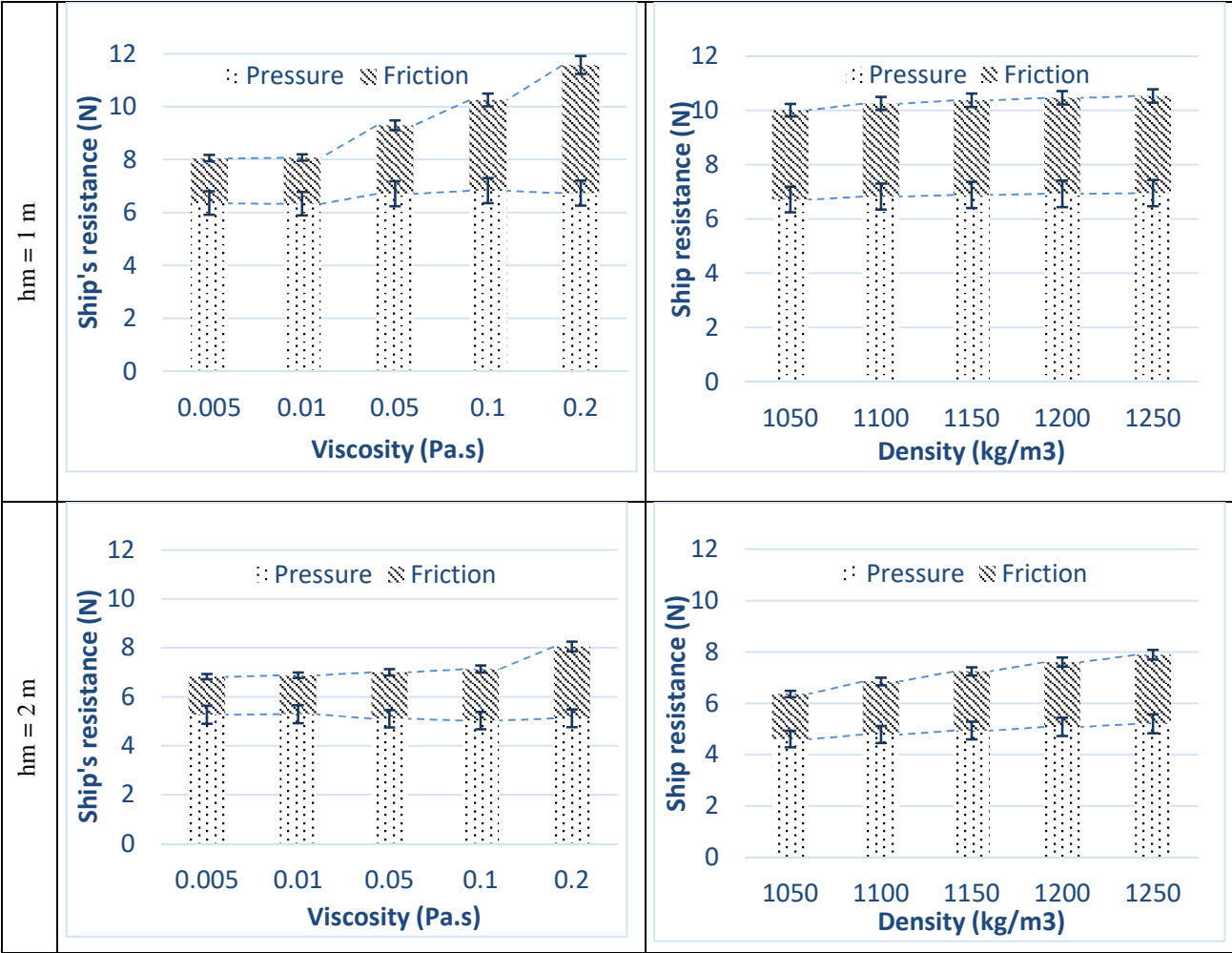


Figure 20. Mud thickness variation for an UKC value of $-10\% * T$.

The computed ship's resistances as a function of the mud viscosity and density were presented in Figure 21 by its two components: wave-making and friction. Basing on these results it was noted that for smaller and medium mud thicknesses the wave-making resistance is dominant compared to the friction resistance, however, for the larger mud thickness, the friction resistance is dominant. This behavior is physical, because it depends on the depth Froude number. Where for high values of depth Froude number the wave-making resistance is dominant while the friction resistance is dominant for very lower values. By analyzing the numerical results of the ship's resistance under the variation of the viscosity, it can be seen that the effect of the later begins to be visible when the viscosity is more than 0.01 Pa.s in smaller and medium mud thicknesses. For the larger mud thickness the effect is visible only when the viscosity of the mud is greater than 0.05 Pa.s. It can also be seen that despite the dominance of the wave-making resistance, its variation at a given mud thickness is insignificant compared to the variation of the friction resistance. Where, the maximum variation of the wave-making resistance is about 30% computed between the largest and the smallest value of the viscosity at the

larger mud thickness. While, the friction resistance was amplified by 2.8, 1.9 and 1.3 times at smaller, medium and larger mud thickness respectively. These behavior is completely realistic for both types of resistances: the friction resistance depends principally on the shear stress on the ship's hull which increases with confinement. However, the wave-making resistance depends on the length and the amplitude of the generated waves which are important when the mud thickness is larger (see figure 16).

Through Figure 21-b, it can be noted that the effect of the density on the ship's resistance is unimportant for the tested thicknesses. The wave-making resistance variation is insignificant at a given mud thickness, whereas, the friction resistance is slightly affected by mud density, where an increase of 23% was computed between the largest and smallest density at the larger mud thickness. This insensitivity to density is related on one side to the non-variation of the generated waves as is illustrated in Figure 12 and on the other hand to the phenomenon of fluidization of the interface of the mud layer caused by the ship passage especially at high speed. This point will be discussed in the next paragraph.



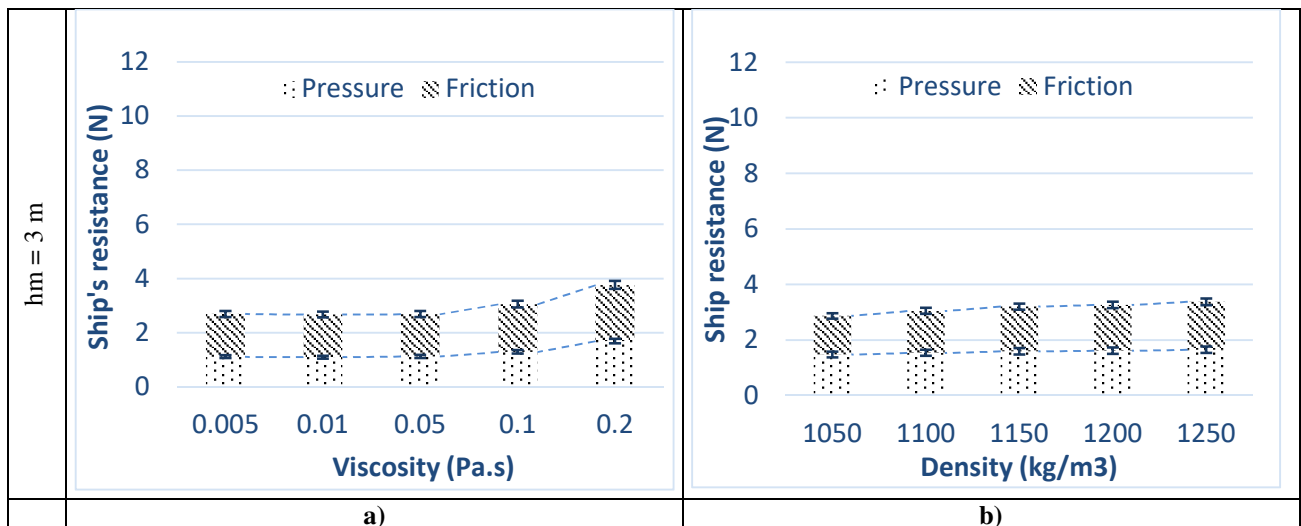


Figure 21. Ship's resistance variation (half of ship) as a function of mud thickness: a) viscosity variation and b) density variation

The second part of this section presents the results for the ship's resistance, studied as a function of the UKC. Mud A was used for 6 values of UKC, as follows: +10%, +5%, 0%, -5 %, -10%, and -15% of the ship's draft. The ship's draft here was 10 m, the mud thickness was 3 m, and the speed of the ship was 10 kn.

From Figure 22, we observe an increase of the total resistance with the decrease of the UKC. The pressure resistance dominates for UKC, varying between +10 and -5%*T. Less than that, the frictional force dominates considerably. We also observe that ship's resistance increase is very slight for UKC values between +5% and -5% and less than -10%. The ship's resistance increase is significant only between +10% and +5%, and between -5% and -10%. By analysing Figure 23-a plotting the area of contact between the hull and the mud, we note that for UKC range of +10%—+5%, the contact area is almost the same and the total resistance increase is principally due to the shallow water effect. For the UKC range -5%—-10%, the resistance increase is principally due to the hull/mud contact. As is shown in Figure 22, the frictional resistance dominates while the pressure resistance increases slightly.

It can also be observed from Figure 23-a that when the ship is sailing inside the mud layer (negative UKC); the keel of the hull is not fully covered by the mud. This is one of the relevant phenomena observed in this work. In fact, when the ship is sailing in the mud, we observe two different behaviours. When the ship's speed is low, the ship's keel is fully covered by the mud. However, when the ship's speed increases, the top boundary of the mud layer tends to be more liquefied, especially at the ship's bow, and a film of very liquefied mud (or turbid water) is created between the mud and

the hull. Figure 23-b, shows the evolution of the hull-mud contact area as a function of the ship's speed (to illustrate
 bitter the contact area, the legend of this figure was limited to a volume of fraction of 0.8)

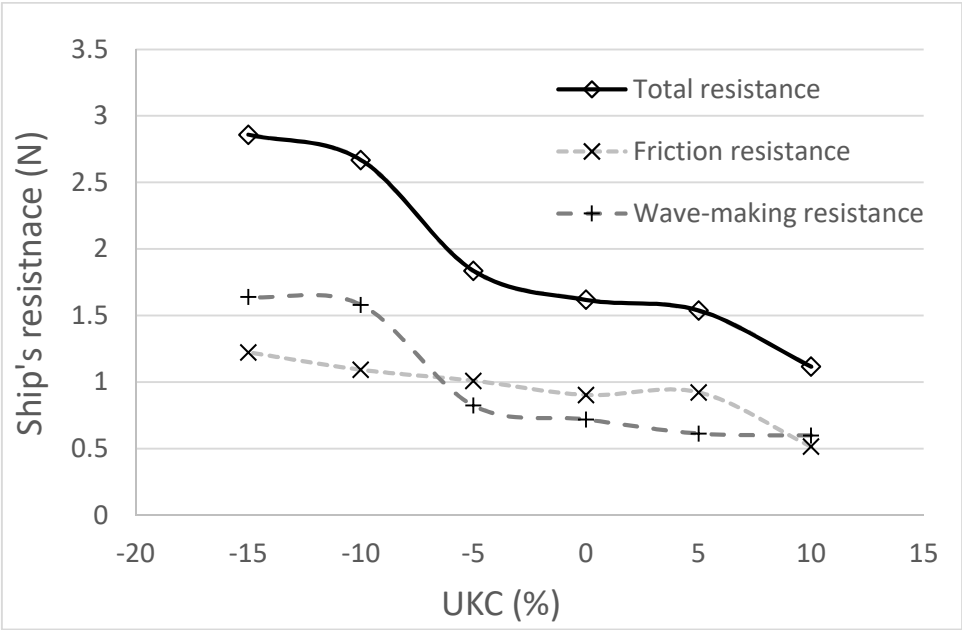


Figure 22. Ship's resistance (half of ship) as a function of UKC (mud A).

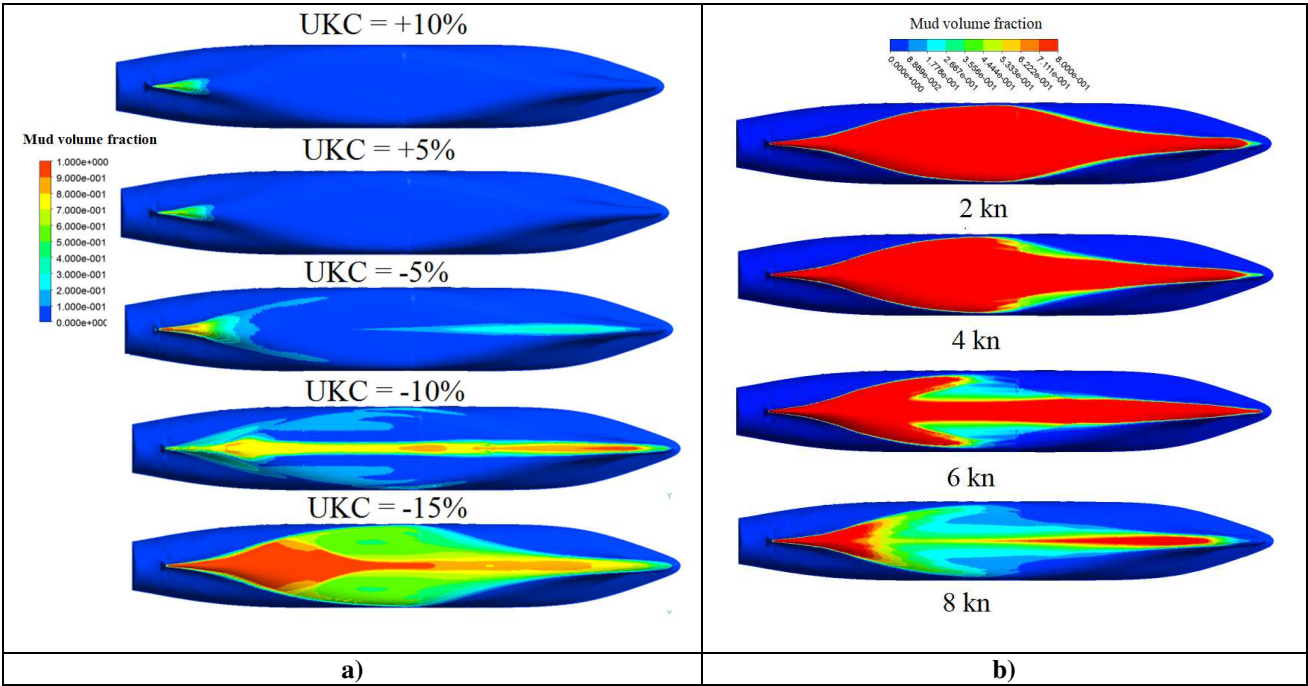


Figure 23. Hull-Mud contact area (mud A): a) as a function of UKC and b) as a function of ship's speed for an UKC of -10%.

4.5 EFFECT OF THE MUDDY SEABED ON THE SHIP'S SQUAT

One of the aims of this work was the numerical study of the influence of the muddy layer on the ship's squat (sinkage and trim). The fluid-structure interaction is treated by a modified Newton algorithm coupled to a steady RANS (Linde et

al., 2016). The standard dynamic Newton algorithm was not used because of several numerical complications encountered. The origin of these complications is essentially the bad estimation of the added mass due to the high blockage coefficient, which considerably affects the stability and convergence of the numerical solution.

Because of the large computation time, only one mud layer thickness was considered (2 m) for an UKC of +10%*T. The effect of the mud properties on the squat was simulated for the four types of mud and for three ship speeds (6, 8, and 10 kn), which correspond to a Froude depth number (Fr_h) of 0.297, 0.396, and 0.495, respectively.

The ship's sinkage as a function of the mud type was plotted in Figure 24 and compared to the experimental and numerical sinkage for a rigid bottom.

Concerning the ship's sinkage, similar observations given by Delefortrie (2016) were noted. First, we observed that the sinkage obtained numerically for a rigid seabed was in accordance with measurements. We also observed that the sinkage increased by increasing the ship's speed in all configurations with or without the mud layer. However, the sinkage values decreased slightly with the change in mud properties. For larger viscosities (Mud C and Mud D), we observed an insignificant decrease, whilst a moderate decrease was observed for Mud A and Mud B. This decrease augmented in turn with the increase in the ship's speed. In fact, this increase was due to the added buoyancy generated by the contact between the hull and the mud. This contact, as mentioned previously, was located at the ship's stern when the undulation crest was larger, as for Mud A and Mud B.

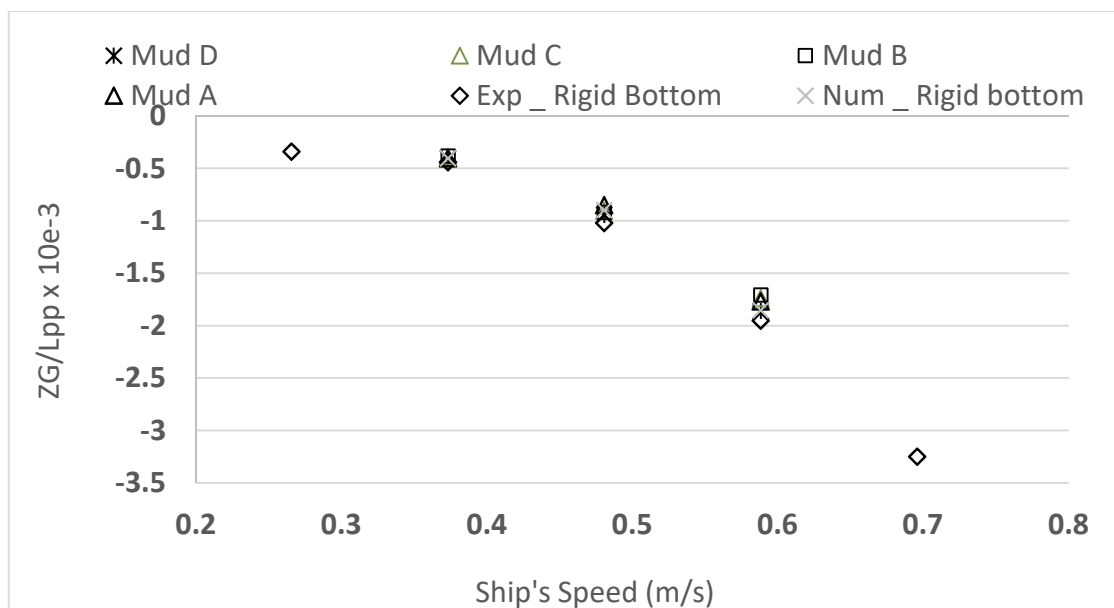


Figure 24. Ship sinkage as a function of the mud properties for an UKC of +10%. Z_G is the sinkage at the mid ship

The ship's trim was plotted in Figure 25. For the selected UKC, the trim has positive values, which correspond to a trim by the stern. The plotted results show that the numerical results are in the same range as measurements without mud. It can also be seen that the mud had an insignificant effect on the trim at low ship speed (6 kn) in the case of Mud B, C, and D. Except in the case of the Mud A, a significant deviation compared to the rigid bottom case was observed. For a ship speed of 10 kn, this deviation decreased, due to the mud-hull contact located at the stern of the ship, which created an asymmetry in the ship's buoyancy. However, the trim behaved differently in the case of Mud D, where the trim deviation (compared to the rigid bottom case) increased with the ship's speed. This increase can be explained by the confinement that this type of mud generates.

Note that some of these observations are not in agreement with observations made by Delefortrie (2016), based on measurements carried out in the towing tank for Manoeuvres in Confined Water at Flanders Hydraulics Research, Antwerp (in Co-operation with Ghent University).

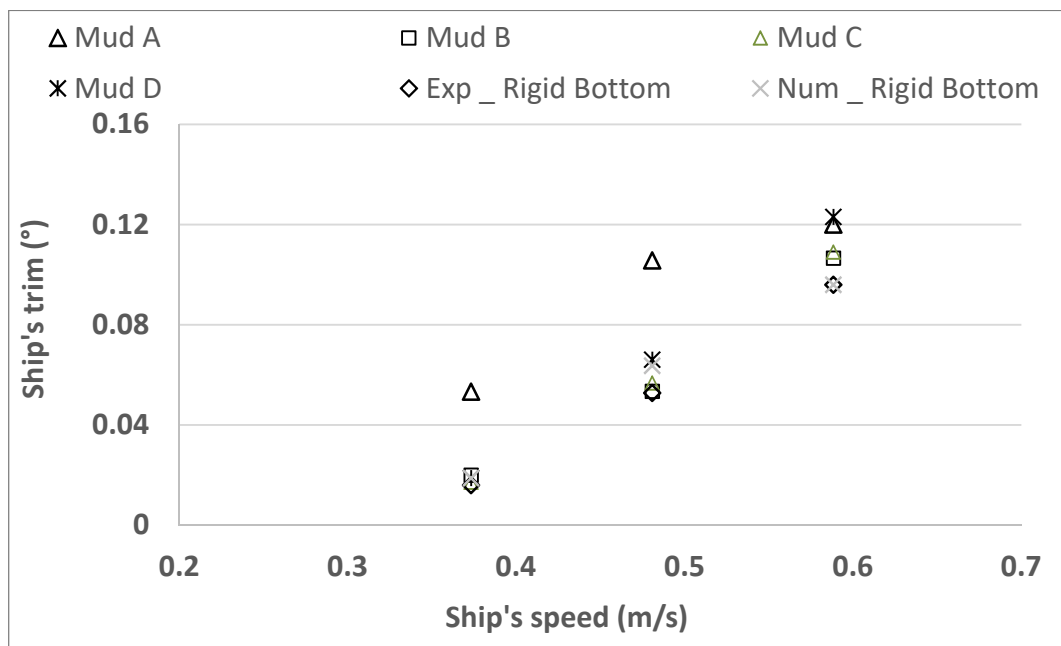


Figure 25. Ship trim as a function of the mud properties for an UKC of +10%.

5 CONCLUSIONS

In this paper, an overview of a numerical investigations on the impact of muddy seabed on a ship's resistance and squat was presented. A multi-phase CFD model was used to estimate the ship's resistance and squat as a function of several parameters: different configurations.

Based on observations noted in the present work, it was concluded the following:

- The obtained numerical results are in agreement with physical models results;
- The internal waves crests depend strongly on the mud properties;
- The internal waves patterns depend strongly on several parameters: the viscosity, the total depth, the UKC and the thickness of the mud layer and the Fr_h is not adapted to characterize the waves pattern.
- The internal waves influence the ship's resistance and squat especially when the UKC is negative;
- The effect of the mud layer on the ship's sinkage is significant only when the UKC is negative;
- The effect of the mud on the ship's resistance can be felt even when the UKC is positive, and this depends on the mud properties;
- The ship's speed tends to move the mud/water interface undulation in the backwards.

The ability of the CFD method to simulate multiphasic flow and interaction between the fluid flow and the structure has been demonstrated. Some difficulties were encountered in the modelling of the depth-dependent density and viscosity of the mud. Some difficulties were also encountered in the simulation of the dynamic ship squat, especially when the mud contacted the ship's hull. An improvement can be made in future works by integrating a new numerical algorithm that stabilises calculations and takes into account the real vertical profile of the density.

6 ACKNOWLEDGEMENTS

The work presented in this paper was performed within the project "Gironde-XL" funded by "Le Grand Port Maritime de Bordeaux" and the European commission.

7 REFERENCES

- AlChang, Y., Zhao, F., Zhang, J., Hong, F.-W., Li, P., Yun, J., 2006. Numerical simulation of internal waves excited by a submarine moving in the two-layer stratified fluid. *J. Hydrodyn. Ser. B* 18, 330–336.
- Crapper, G.D., 1967. Ship waves in a stratified ocean. *J. Fluid Mech.* 29, 667–672.

616 Debaillon, P., 2010. Numerical investigation to predict ship squat. *J. Sh. Res.* 54, 133–140.
 617 Delefortrie, G., 2016. Ship Manoeuvring Behaviour in Muddy Navigation Areas, in: *Proceedings of 4th MASSHCON*.
 618 pp. 26–36. <https://doi.org/10.18451/978-3-939230-38-0>
 619 Delefortrie, G., Vantorre, M., 2005. Modelling navigation in muddy areas, *Hydronav'05 - Manoeuvring '05: Joint 16th*
 620 *International Conference on Hydrodynamics in Ship Design and 3rd International Symposium on Ship*
 621 *Manoeuvring*, Ostróda, Poland, September 2005.
 622 Delefortrie, G., Vantorre, M., Eloot, K., 2004. Linear manoeuvring derivatives in muddy navigation areas. *Trans. R.*
 623 *Inst. Nav. Archit. Int. J. Marit. Eng.* 146, 1–13.
 624 Eloot, K., Delefortrie, G., Vantorre, M., Quadvlieg, F., 2015. Validation of ship manoeuvring in shallow water through
 625 free-running tests, in: *Proceedings of the ASME 2015 34th International Conference on Ocean, Offshore and*
 626 *Arctic Engineering*.
 627 Esmaeilpour, M., Martin, J.E., Carrica, P.M., 2016. Near-field flow of submarines and ships advancing in a stable
 628 stratified fluid. *Ocean Eng.* 123, 75–95.
 629 Gourlay, T., 2008. Slender-body methods for predicting ship squat. *Ocean Eng.* 35, 191–200.
 630 Hudimac, A.A., 1961. Ship waves in a stratified ocean. *J. Fluid Mech.* 11, 229–243.
 631 ITTC, 2011. ITTC – Recommended Procedures and Guidelines - Verification and validation of linear and weakly
 632 nonlinear seakeeping computer codes. 7.5-02-07-02.5 (Revision 01) 17.
 633 Kaidi, S., Smaoui, H., Sergent, P., Daly, F., 2018. Numerical investigation of the impact of the inland transport on bed
 634 erosion and transport of suspended sediment : propulsive system and confinement effect. *PIANC-World Congress*,
 635 Panama, pp. 0–12.
 636 Kaidi, S., Smaoui, H., Sergent, P., 2018. CFD Investigation of Mutual Interaction between Hull , Propellers , and
 637 Rudders for an Inland Container Ship in Deep , Very Deep , Shallow , and Very Shallow Waters. *J. Waterw. Port,*
 638 *Coastal, Ocean Eng.* 144. [https://doi.org/10.1061/\(ASCE\)WW.1943-5460.0000458](https://doi.org/10.1061/(ASCE)WW.1943-5460.0000458).
 639 Kaidi, S., Smaoui, H., Sergent, P., 2017. Numerical estimation of bank-propeller-hull interaction effect on ship
 640 manoeuvring using CFD method. *J. Hydrodyn.* 29. [https://doi.org/10.1016/S1001-6058\(16\)60727-8](https://doi.org/10.1016/S1001-6058(16)60727-8)
 641 Linde, F., Ouahsine, A., Huybrechts, N., Sergent, P., 2016. Three-dimensional numerical simulation of ship resistance in
 642 restricted waterways: Effect of ship sinkage and channel restriction. *J. Waterw. Port, Coastal, Ocean Eng.*
 643 6016003.
 644 Ma, C., Zhang, C., Chen, X., Jiang, Y., Noblesse, F., 2016. Practical estimation of sinkage and trim for common generic
 645 monohull ships. *Ocean Eng.* 126, 203–216.

- Mucha, P., el Moutar, O., Böttner, C.-U., 2014. Technical Note: PreSquat – Workshop on Numerical Prediction of Ship Squat in Restricted Waters. *Sh. Technol. Res.* 61, 162–165.
- Razgallah, I., Kaidi, S., Smaoui, H., Sergent, P., 2018. The impact of free surface modelling on hydrodynamic forces for ship navigating in inland waterways: water depth, drift angle, and ship speed effect. *J. Mar. Sci. Technol.* <https://doi.org/10.1007/s00773-018-0566-y>
- Sergent, P., Lefrançois, E., Mohamad, N., 2015. Virtual bottom for ships sailing in restricted waterways (unsteady squat). *Ocean Eng.* 110, 205–214.
- Stern, F., 2013. Computational ship hydrodynamics: nowadays and way forward. *Int. Sh. Build Prog.* 60, 3–105.
- Tezdogan, T., Incecik, A., Turan, O., 2016. Full-scale unsteady RANS simulations of vertical ship motions in shallow water. *Ocean Eng.* 123, 131–145.
- Tuck, E.O., 1964. A systematic asymptotic expansion procedure for slender ships. *J. Sh. Res.* 8, 15–23.
- Tulin, M.P., Yao, Y., Wang, P., 2000. The generation and propagation of ship internal waves in a generally stratified ocean at high densimetric Froude numbers, including nonlinear effects. *J. Sh. Res.* 44, 197–227.
- Wurpts, R.W., 2005. 15 years experience with fluid mud: Definition of the nautical bottom with rheological parameters. *Terra Aqua* 22–32.
- Wurpts, R., 2005. 15 years' experience with fluid mud: definition of the nautical bottom with rheological parameters. *Terra et Aqua.* 99
- Zhao, F., Zhang, J., Hong, F.-W., Li, P., Yun, J., 2006. Numerical simulation of internal waves excited by a submarine moving in the two-layer stratified fluid. *J. Hydrodyn. Ser. B* 18, 330–336.

8 AUTHORS BIOGRAPHY

Sami Kaidi holds the current position of researcher at Centre for Studies and Expertise on Risks, Environment, Mobility, and Urban and Country Planning. Hi is responsible for Ship Hydrodynamic and Manoeuvring researches. His previous experience includes: CFD method; Fluid-structure interaction, numerical methods,

Emmanuel Lefrançois holds the current position of Professor at University of Technology of Compiègne. Hi is responsible for Fluid-structure interaction researches. His previous experience includes: the fluid-structure interaction methods and the development of innovative numerical methods for engineering problems.

675 **Hassan Smaoui** holds the current position of research director at Centre for Studies and Expertise on Risks, Environ-
676 ment, Mobility, and Urban and Country Planning. He is responsible for laboratory of numerical hydraulic. His previous
677 experience includes: the sedimentary transport, the bank erosion and finite element method.